Radiative lepton flavor violating B, D, and K decays

Derek Hazard[1] and Alexey A. Petrov[1,2]

[1]Department of Physics and Astronomy Wayne State University, Detroit, Michigan 48201, USA
[2]Michigan Center for Theoretical Physics University of Michigan, Ann Arbor, Michigan 48196, USA

(Received 15 December 2017; published 20 July 2018)

We argue that radiative lepton flavor violating (RLFV) decays $P \to \gamma \ell_1 \bar{\ell}_2$ of $P = B_q^0$, $\bar{D}^0$, and K^0 meson states are robust probes of new physics models. In particular, they could be used to put constraints on the Wilson coefficients of effective operators describing lepton flavor-changing neutral current interactions at low energy scales. We set up a generic framework for describing these transitions and review new physics constraints from $P \to \ell_1 \bar{\ell}_2$ decays. There is discussion of how RLFV transitions provide access to the operators that cannot be constrained in two-body decays and we in turn motivate further experimental searches via these channels.

DOI: 10.1103/PhysRevD.98.015027

I. INTRODUCTION

Currently operating and future B-factories, such as LHCb and Belle-II, will be accumulating significant amounts of beauty and charm decay data. These large data sets will be quite useful in studies of extremely small decay rates of B and D mesons, which could probe new physics (NP) at unprecedentedly high energy scales. In particular, studies of pseudoscalar meson decays $P = B_q^0$, $\bar{D}^0$, and K^0 into the final states containing charged leptons of different flavors such as $P \to \ell_1 \bar{\ell}_2$ and $P \to \gamma \ell_1 \bar{\ell}_2$ could be performed. Such decays are induced by the operators that generate flavor-changing neutral currents (FCNC) in the lepton sector, which provide a fruitful approach to probing beyond the standard model (BSM) physics, assuming of course that such flavor-violating interactions are allowed in the BSM models. There are indeed many well-established new physics models (see, e.g., [1–7]) that meet this opportunity and predict charged lepton flavor violating (CLFV) transition rates that are significantly larger than the standard model (SM) rates [1].

A convenient way to describe CLFV transitions in low energy experiments is by introducing an effective Lagrangian, $\mathcal{L}_{\rm eff}$. Such a Lagrangian is a convenient parametrization of all new physics models that include lepton flavor violation with the details of the models encoded in the Wilson coefficients (WCs) of $\mathcal{L}_{\rm eff}$, which are obtained by matching the effective Lagrangian to a given BSM model at the new physics scale Λ [8]. This Lagrangian is required to be invariant under the unbroken symmetry groups $SU(3)_c \times U(1)_{\rm em}$ below the electroweak symmetry breaking scale. At the low scale for which a given process occurs the effective operators would exhibit the relevant standard model (SM) degrees of freedom with the effective operators written completely using quarks ($q_i = b$, c, s, u, and d) and leptons ($\ell_i = \tau$, μ, and e). In what follows, we assume that top quarks are integrated out of the theory, and we do not consider neutrinos. The effective Lagrangian $\mathcal{L}_{\rm eff}$ that involves CLFV can be written as

$$\mathcal{L}_{\rm eff} = \mathcal{L}_{\ell q} + \mathcal{L}_D + \cdots, \tag{1}$$

where $\mathcal{L}_D$ is a dipole part, $\mathcal{L}_{\ell q}$ is the part that contains four-fermion interactions, and the ellipses represent parts of the Lagrangian not relevant to this work. Since here we are interested in the decays of electrically-neutral pseudoscalar B_q^0, $\bar{D}^0$, and K^0 mesons to flavor-off-diagonal lepton pairs and other particles, the transitions involve FCNC interactions on both quark and lepton sides. We neglect to include the gluonic part of the Lagrangian, $\mathcal{L}_{\mathcal{G}}$, here as it's contributions for B_q^0, D^0, and K^0 mesons is a loop process one order beyond this work and therefore highly suppressed. It would be included for the case of quarkonium decays as seen in Ref. [9]. This can be understood by considering the wave function of quarkonia which includes $q\bar{q}$ quark pairs of the same flavor as well as a significant gluon content, while the wave functions of mesons such as B_q^0, D^0, and K^0 are composed of $q_1\bar{q}_2$ quark pairs of different flavors.

The dipole part of Eq. (1), which could contribute to the radiative decays $P \to \gamma \ell_1 \bar{\ell}_2$ is written as [10]

$$\mathcal{L}_D = -\frac{m_2}{\Lambda^2}[(C_{DR}^{\ell_1\ell_2}\bar{\ell}_1\sigma^{\mu\nu}P_L\ell_2 + C_{DL}^{\ell_1\ell_2}\bar{\ell}_1\sigma^{\mu\nu}P_R\ell_2)F_{\mu\nu} + \text{H.c.}]. \quad (2)$$

The WCs of $\mathcal{L}_D$ have been well constrained in leptonic LFV decays [1].

Note that it is known that the quark FCNC transitions, at least in the decays of down-type quarks, are dominated by the SM contributions. For instance, the dipole operator describing $q_1 \to q_2\gamma$ can be written as [11]

$$\mathcal{L}_{\text{peng}} = \frac{G_F}{\sqrt{2}}\sum_q \lambda_q^P C_{7\gamma}\frac{\sqrt{4\pi\alpha}}{\pi^2}\frac{m_{q_1}}{2}\bar{q}_1\sigma_{\mu\nu}(1+\gamma_5)F^{\mu\nu}q_2 + \text{H.c.} \quad (3)$$

Here $\lambda_q^P = V_{qq_2}V_{qq_1}^*$ denotes the appropriate Cabibbo-Kobayashi-Maskawa (CKM) matrix elements, m_{q_1} is the heavier quark, and $C_{7\gamma}$ is the corresponding Wilson coefficient [11].

The four-fermion dimension-six lepton-quark part of the effective Lagrangian, Eq. (1), takes the form [10]:

$$\begin{aligned}\mathcal{L}_{\ell q} = -\frac{1}{\Lambda^2}\sum_{q_1,q_2}[&(C_{VR}^{q_1q_2\ell_1\ell_2}\bar{\ell}_1\gamma^\mu P_R\ell_2 + C_{VL}^{q_1q_2\ell_1\ell_2}\bar{\ell}_1\gamma^\mu P_L\ell_2)\bar{q}_1\gamma_\mu q_2 + (C_{AR}^{q_1q_2\ell_1\ell_2}\bar{\ell}_1\gamma^\mu P_R\ell_2 + C_{AL}^{q_1q_2\ell_1\ell_2}\bar{\ell}_1\gamma^\mu P_L\ell_2)\bar{q}_1\gamma_\mu\gamma_5 q_2 \\ &+ m_2 m_{q_H} G_F(C_{SR}^{q_1q_2\ell_1\ell_2}\bar{\ell}_1 P_L\ell_2 + C_{SL}^{q\ell_1\ell_2}\bar{\ell}_1 P_R\ell_2)\bar{q}_1 q_2 + m_2 m_{q_H} G_F(C_{PR}^{q_1q_2\ell_1\ell_2}\bar{\ell}_1 P_L\ell_2 + C_{PL}^{q_1q_2\ell_1\ell_2}\bar{\ell}_1 P_R\ell_2)\bar{q}_1\gamma_5 q_2 \\ &+ m_2 m_{q_H} G_F(C_{TR}^{q_1q_2\ell_1\ell_2}\bar{\ell}_1\sigma^{\mu\nu}P_L\ell_2 + C_{TL}^{q_1q_2\ell_1\ell_2}\bar{\ell}_1\sigma^{\mu\nu}P_R\ell_2)\bar{q}_1\sigma_{\mu\nu}q_2 + \text{H.c.}].\end{aligned} \quad (4)$$

Here m_{q_H} is the mass of the heavier quark ($m_{q_H} = \max[m_{q_1}, m_{q_2}]$) and $P_{R,L} = (1 \pm \gamma_5)/2$ is the right (left) chiral projection operator. In general the Wilson coefficients would be different for different lepton flavors ℓ_i and quark flavors q_i. Note that, contrary to some previous studies, we include tensor operator in Eq. (4) (see [9] for motivation). CP-conservation is assumed so all the Wilson coefficients in Eq. (4) should be viewed as real numbers.

In this paper we discuss the possibility of the Wilson coefficients of the effective Lagrangian in Eq. (1) for different ℓ_i and q_i be determined from experimental data on leptonic and radiative leptonic CLFV decays of B_q^0, $\bar{D}^0$, and K^0 states. We review two-body decays $P \to \ell_1\bar{\ell}_2$ in Sec. III. We will note that restricted kinematics of the two-body transitions would allow us to select operators with particular quantum numbers significantly reducing the reliance on the single operator dominance assumption [9]. The main part of the paper, Sec. III, will be devoted to discussion of radiative lepton-flavor violating (RLFV) decays $P \to \gamma\ell_1\bar{\ell}_2$. We will summarize our results in Sec. IV and conclude in Sec. V.

Note that here we only consider short distance effects in kaon decays. In the SM long distance effects on decays such as $K_{L(S)}^0 \to \gamma\ell\bar{\ell}$ dominate the dynamics [12]. In light of this, our kaon results may be modified by long distance effects.

In what follows, we will use the convention that the subscript of "1" will denote the lighter lepton and the subscript "2" will denote the heavier lepton. Unless otherwise specified when studying the branching ratios we assume for a meson, P, that $\mathcal{B}(P \to (\gamma)\ell_1\ell_2) = \mathcal{B}(P \to (\gamma)\bar{\ell}_1\ell_2) + \mathcal{B}(P \to (\gamma)\ell_1\bar{\ell}_2)$. Finally, it is important to note that some of the two-body and all of the three-body transitions have yet to be experimentally studied. Numerical constraints on some Wilson coefficients of the effective Lagrangian, $\mathcal{L}_{\text{eff}}$, from these unstudied decays are not available.

II. TWO-BODY DECAYS $P \to \ell_1\bar{\ell}_2$

Many studies have focused on rare leptonic decays of B_q^0 mesons, $B_q \to \ell\bar{\ell}$, as both precision tests of the SM and as an opportunity to search for new physics (e.g., [13–17]). The abundance of produced B_q^0 and $\bar{D}^0$ states at the LHCb, Belle II, and BESIII experiments also allows for studies of lepton-flavor violating decays at these experiments [18,19]. Such decays were discussed at length previously, mainly in the context of particular models. Here we shall review these transitions emphasizing the possibility to constrain Wilson coefficients of the axial and pseudoscalar operators of the effective Lagrangian in Eq. (1). These decays would provide information about $C_{PL}^{q_1q_2\ell_1\ell_2}(C_{PR}^{q_1q_2\ell_1\ell_2})$ and/or $C_{AL}^{q_1q_2\ell_1\ell_2}(C_{AR}^{q_1q_2\ell_1\ell_2})$ in Eq. (4). One can write the most general expression for the $P \to \ell_1\bar{\ell}_2$ decay amplitude as [9]

$$\mathcal{A}(P \to \ell_1\bar{\ell}_2) = \bar{u}(p_1, s_1)[E_P^{q_1q_2\ell_1\ell_2} + iF_P^{q_1q_2\ell_1\ell_2}\gamma_5]v(p_2, s_2) \quad (5)$$

with $E_P^{q_1q_2\ell_1\ell_2}$ and $F_P^{q_1q_2\ell_1\ell_2}$ being dimensionless constants which depend on the Wilson coefficients of operators in Eq. (1) and various decay constants.

The amplitude of Eq. (5) leads to the branching ratio for flavor off-diagonal leptonic decays of pseudoscalar mesons:

$$\mathcal{B}(P \to \ell_1\bar{\ell}_2) = \frac{m_P}{8\pi\Gamma_P}(1-y^2)^2[|E_P^{q_1q_2\ell_1\ell_2}|^2 + |F_P^{q_1q_2\ell_1\ell_2}|^2]. \quad (6)$$

TABLE I. Available experimental limits on $\mathcal{B}(P \to \ell_1 \bar{\ell}_2)$ [19,21–24]. Center dots signify that no experimental data are available; "FPS" means that the transition is forbidden by phase space.

$\ell_1\ell_2$	$\mu\tau$	$e\tau$	$e\mu$
$\mathcal{B}(B_d^0 \to \ell_1\ell_2)$	2.2×10^{-5}	2.8×10^{-5}	1.0×10^{-9}
$\mathcal{B}(B_s^0 \to \ell_1\ell_2)$	⋯	⋯	5.4×10^{-9}
$\mathcal{B}(\bar{D}^0 \to \ell_1\ell_2)$	FPS	⋯	1.3×10^{-8}
$\mathcal{B}(K_L^0 \to \ell_1\ell_2)$	FPS	FPS	4.7×10^{-12}

TABLE II. Pseudoscalar meson decay constants [25,26], total decay widths, and meson masses [19] used in the calculation of branching ratios $\mathcal{B}(P \to \ell_1 \bar{\ell}_2)$.

State	B_d^0	B_s^0	$\bar{D}^0$	K_L^0
f_P, MeV	186 ± 4	224 ± 4	207.4 ± 3.8	155.0 ± 1.9
Γ_P, 10^{-14} MeV	4330 ± 11	4374 ± 15	16050 ± 60	1.287 ± 0.005
m_P, GeV	5.28	5.37	1.86	0.498

TABLE III. Constraints on the Wilson coefficients from pseudoscalar meson decays. Note the K_L^0 results only include short distance effects. Center dots signify that no experimental data are available to produce a constraint; "FPS" means that the transition is forbidden by phase space. Particle masses and other input parameters are from [19,21–24].

Wilson coefficient	Leptons $\ell_1\ell_2$	Initial state $B_d^0(d\bar{b})$	$B_s^0(s\bar{b})$	$\bar{D}^0(u\bar{c})$	$K_L^0((d\bar{s} - s\bar{d})/\sqrt{2})$
$\lvert C_{AL}^{q_1q_2\ell_1\ell_2}/\Lambda^2\rvert$	$\mu\tau$	2.3×10^{-8}	⋯	FPS	FPS
	$e\tau$	2.6×10^{-8}	⋯	⋯	FPS
	$e\mu$	2.3×10^{-9}	4.4×10^{-9}	2.4×10^{-8}	5.0×10^{-12}
$\lvert C_{AR}^{q_1q_2\ell_1\ell_2}/\Lambda^2\rvert$	$\mu\tau$	2.3×10^{-8}	⋯	FPS	FPS
	$e\tau$	2.6×10^{-8}	⋯	⋯	FPS
	$e\mu$	2.3×10^{-9}	4.4×10^{-9}	2.4×10^{-8}	5.0×10^{-12}
$\lvert C_{PL}^{q_1q_2\ell_1\ell_2}/\Lambda^2\rvert$	$\mu\tau$	7.1×10^{-5}	⋯	FPS	FPS
	$e\tau$	8.0×10^{-5}	⋯	⋯	FPS
	$e\mu$	7.1×10^{-6}	1.3×10^{-5}	5.9×10^{-4}	1.7×10^{-6}
$\lvert C_{PR}^{q_1q_2\ell_1\ell_2}/\Lambda^2\rvert$	$\mu\tau$	7.1×10^{-5}	⋯	FPS	FPS
	$e\tau$	8.0×10^{-5}	⋯	⋯	FPS
	$e\mu$	7.1×10^{-6}	1.3×10^{-5}	5.9×10^{-4}	1.7×10^{-6}

Here Γ_P is the total width of the pseudoscalar state. We have once again neglected the mass of the lighter lepton and set $y = m_2/m_P$. Calculating $E_P^{q_1q_2\ell_1\ell_2}$ and $F_P^{q_1q_2\ell_1\ell_2}$ for $P = B_d^0$ $(q_1q_2 = db)$, B_s^0 $(q_1q_2 = sb)$, $\bar{D}^0$ $(q_1q_2 = cu)$, and, K_L^0 $(q_1q_2 = ds)$, the coefficients are

$$\begin{aligned} E_P^{q_1q_2\ell_1\ell_2} &= \kappa_P \frac{m_P f_P y}{2\Lambda^2}[(C_{AL}^{q_1q_2\ell_1\ell_2} + C_{AR}^{q_1q_2\ell_1\ell_2}) \\ &\quad + m_P^2 G_F (C_{PL}^{q_1q_2\ell_1\ell_2} + C_{PR}^{q_1q_2\ell_1\ell_2})], \\ F_P^{q_1q_2\ell_1\ell_2} &= i\kappa_P \frac{m_P f_P y}{2\Lambda^2}[(C_{AL}^{q_1q_2\ell_1\ell_2} - C_{AR}^{q_1q_2\ell_1\ell_2}) \\ &\quad + m_P^2 G_F (C_{PL}^{q_1q_2\ell_1\ell_2} - C_{PR}^{q_1q_2\ell_1\ell_2})]. \end{aligned} \tag{7}$$

The hadronic matrix element[1] in Eq. (7) is defined as [20]

$$\langle 0|\bar{q}_1\gamma^\mu\gamma_5 q_2|P(p)\rangle = -if_P p^\mu. \tag{8}$$

Here p is the momentum of the meson. The constant κ_P is 1 for B_q^0, $\bar{D}^0$, and K^0; and $1/\sqrt{2}$ for $K_{L(S)}^0$. The experimental limits and numerical values of the pseudoscalar decay constants used in the calculations can be found in

[1]One could also consider similar matrix elements with vector and tensor currents, but it can be shown that these are zero by applying parity $\hat{\mathcal{P}}$ and time reversal $\hat{\mathcal{T}}$ operators to the matrix elements (e.g., $\langle 0|\bar{q}_1\gamma^\mu q_2|P(p)\rangle = \langle 0|\hat{\mathcal{T}}^{-1}\hat{\mathcal{P}}^{-1}\hat{\mathcal{P}}\hat{\mathcal{T}}\bar{q}_1\gamma^\mu q_2\hat{\mathcal{T}}^{-1}\hat{\mathcal{P}}^{-1}\hat{\mathcal{P}}\hat{\mathcal{T}}|P(p)\rangle = -\langle 0|\bar{q}_1\gamma^\mu q_2|P(p)\rangle = 0$).

Tables I and II. The resulting constraints on the Wilson coefficients are found in Table III.

III. THREE-BODY RADIATIVE DECAYS $P \to \bar{\ell}_1 \ell_2 \gamma$

Similarly to the $B_s^0 \to \mu^+\mu^-\gamma$ transition [27–32], addition of a photon to the $\ell_1\bar{\ell}_2$ final state allows one to probe operators of the effective Lagrangian that do not contribute to $P \to \ell_1\bar{\ell}_2$ transition. This was pointed out for the LFV decays in [9], and, more importantly in [33] (for a calculation of $B_s^0 \to \ell_1\bar{\ell}_2\gamma$ in the model of [34]). In addition, $P \to \ell_1\bar{\ell}_2$ decays suffer from chiral suppression [see Eq. (7)], which three-body radiative decays do not necessarily exhibit. Thus, it is possible that RLFV decays might have larger branching ratios than two-body LFV transitions (see [27–32] for similar effects in lepton flavor conserving decays). Here we evaluate radiative lepton-flavor violating decays of the pseudoscalar mesons with the model-independent effective Lagrangian of Eq. (1).

It might be theoretically easier to deal with a three-body final state that contains no strongly-interacting composite particles. Still, the calculation of the $P \to \ell_1\bar{\ell}_2\gamma$ decay is more complicated than $P \to \ell_1\bar{\ell}_2$, where all nonperturbative effects are summarized in one decay constant f_P. Further, because of the electromagnetic gauge invariance, it is important to have a good understanding of what kind of constraints the kinematic structure of the decay amplitude imposes on the dynamics of these transitions. Let us now derive the most general amplitude for $P \to \ell_1\bar{\ell}_2\gamma$.

A. General amplitude and differential decay rate for $P \to \bar{\ell}_1\ell_2\gamma$

The most general expression for the $P(p) \to \gamma(k)\ell_1(p_1)\bar{\ell}_2(p_2)$ decay amplitude can be obtained using the Bardeen-Tung formalism [35]. The decay amplitude can be written as

$$A(P(p) \to \gamma(k)\ell_1(p_1)\bar{\ell}_2(p_2)) = \bar{u}(p_1, s_1)M^\mu(p, k, q)v(p_2, s_2)\varepsilon^*_\mu(k), \quad (9)$$

where $\bar{u}(p_1, s_1)$ and $v(p_2, s_2)$ are spinors for ℓ_1 and $\bar{\ell}_2$, $q = \frac{1}{2}(p_1 - p_2)$, and $\varepsilon^*_\mu(k)$ is the polarization vector of the photon. The function $M^\mu(p, k, q)$, which we seek to parametrize, transforms as a tensor under Lorentz transformations. This function should only contain dynamical singularities, so particular care should be taking by writing it in such a way that it does not contain kinematical ones. The most general expression for the $M^\mu(p, k, q)$ from Eq. (9) can be written by expanding it into simpler Lorentz structures $\ell_i^\mu(p, q, k)$ multiplied by the invariant functions $M_i^{P\ell_1\ell_2}$, which only depend on Lorentz invariants,

$$M^\mu(p, k, q) = \sum_i \ell_i^\mu(p, q, k)M_i^{P\ell_1\ell_2}(p^2, \ldots). \quad (10)$$

The most general parametrization of Eq. (10) contains twelve form-factors,

$$\begin{aligned} M^\mu(p, k, q) &= \gamma^\mu(M_1^{P\ell_1\ell_2} + \not{k}M_2^{P\ell_1\ell_2}) + i\gamma_5\gamma^\mu(M_3^{P\ell_1\ell_2} + \not{k}M_4^{P\ell_1\ell_2}) \\ &+ q^\mu(M_5^{P\ell_1\ell_2} + \not{k}M_6^{P\ell_1\ell_2}) + i\gamma_5 q^\mu(M_7^{P\ell_1\ell_2} + \not{k}M_8^{P\ell_1\ell_2}) \\ &+ p^\mu(M_9^{q\ell_1\ell_2} + \not{k}M_{10}^{q\ell_1\ell_2}) + i\gamma_5 p^\mu(M_{11}^{P\ell_1\ell_2} + \not{k}M_{12}^{P\ell_1\ell_2}). \end{aligned} \quad (11)$$

In the writing of Eq. (11) we used the equation of motion for the lepton spinors, and rewrote terms containing $\sigma^{\mu\nu}$ in terms of components, e.g., $i\sigma^{\mu\nu}q_\nu = q^\mu - \gamma^\mu\not{q}$ and $\sigma^{\mu\nu}\gamma_5 q_\nu = iq^\mu\gamma_5 - i\gamma^\mu\not{q}\gamma_5$. Note that terms proportional to $\not{q}$ can be expressed as terms proportional to $\not{k}$ using momentum conservation and equations of motion. Next, terms proportional to the $\epsilon^{\mu\nu\alpha\beta}$ tensor, such as $\epsilon^{\mu\nu\alpha\beta}\gamma_\nu p_\alpha k_\beta$, can be written in terms of the existing form factors of Eq. (11) using the relation

$$i\epsilon^{\mu\nu\alpha\beta}\gamma_\beta = \gamma^\mu\gamma^\nu\gamma^\alpha\gamma_5 - g^{\mu\nu}\gamma^\alpha\gamma_5 - g^{\nu\alpha}\gamma^\mu\gamma_5 + g^{\mu\alpha}\gamma^\nu\gamma_5 \quad (12)$$

and the equations of motion. Finally, all possible terms in Eq. (11) proportional to k^μ trivially vanish by gauge invariance.

The set of Eq. (11) is still not minimal, as the condition of gauge invariance $k_\mu M^\mu(p, k, q) = 0$ implies that some of the $M_i^{P\ell_1\ell_2}$ in Eq. (11) are not independent. An elegant way of finding the minimal set of gauge-invariant Lorentz structures has been given in [35], which we shall apply to our analysis. To get the minimal set, it is most convenient to apply a projection operator

$$P^{\mu\nu} = g^{\mu\nu} - \frac{p^\mu k^\nu}{(p \cdot k)} \quad (13)$$

to $M^\mu(p, k, q)$. Since $P^{\mu\nu}M_\nu = M^\mu$ and $k_\mu P^{\mu\nu} = 0$, $P^{\mu\nu}$ does indeed project out gauge-invariant structures in $M^\mu(p, k, q)$. Applying $P^{\mu\nu}$ to Eq. (11) we learn that terms proportional to p^μ do not give contributions to the minimal set and should be dropped, leaving the number of independent amplitudes at eight.[2] Applying the condition $k_\mu\ell_i^\mu = 0$ and eliminating kinematical singularities we write the Lorentz structures L_i^μ for the set of amplitudes as

$$M^\mu(p, k, q) = \sum_i L_i^\mu(p, q, k)A_i^{P\ell_1\ell_2}(p^2, \ldots), \quad (14)$$

[2]The number of linearly independent amplitudes is equal to the number of helicity states [36–39]. There are two possible helicity states for the leptons, down or up ($\Leftarrow$ or $\Rightarrow$), and two for the photon, minus or plus ($\leftarrow$ or $\rightarrow$). For the $P \to \bar{\ell}_1\ell_2\gamma$ decay this yields $2 \times 2 \times 2 = 8$ possible combinations: $\leftarrow\Rightarrow\Rightarrow$ ($L = 0$), $\rightarrow\Leftarrow\Leftarrow$ ($L = 0$), $\leftarrow\Leftarrow\Rightarrow$ ($L = 1$), $\leftarrow\Rightarrow\Leftarrow$ ($L = 1$), $\rightarrow\Leftarrow\Rightarrow$ ($L = 1$), $\rightarrow\Rightarrow\Leftarrow$ ($L = 1$), $\rightarrow\Rightarrow\Rightarrow$ ($L = 2$), and $\leftarrow\Leftarrow\Leftarrow$ ($L = 2$). Here L is the orbital angular momentum allowed for each helicity state due to conservation of total angular momentum ($J = 0$).

which are defined in a manner that removes all kinematical singularities. The $A_i^{P\ell_1\ell_2}(p^2,\ldots)$ are new scalar form factors, while L_i^μ are

$$\begin{aligned}
L_1^\mu &= \gamma^\mu \not{k}, \qquad L_2^\mu = i\gamma_5\gamma^\mu \not{k},\\
L_3^\mu &= (p\cdot k)q^\mu - (k\cdot q)p^\mu,\\
L_4^\mu &= i\gamma_5[(p\cdot k)q^\mu - (k\cdot q)p^\mu],\\
L_5^\mu &= (p\cdot k)\gamma^\mu - p^\mu \not{k},\\
L_6^\mu &= i\gamma_5[(p\cdot k)\gamma^\mu - p^\mu \not{k}],\\
L_7^\mu &= q^\mu \not{k} - (k\cdot q)\gamma^\mu,\\
L_8^\mu &= i\gamma_5[q^\mu \not{k} - (k\cdot q)\gamma^\mu].
\end{aligned} \tag{15}$$

This implies that the decay amplitude can be written as

$$\begin{aligned}
&A(P(p)\to\gamma(k)\ell_1(p_1)\bar{\ell}_2(p_2))\\
&\quad=\sum_i A_i^{P\ell_1\ell_2}(p^2,\ldots)\bar{u}(p_1,s_1)L_i^\mu(p,q,k)v(p_2,s_2)\varepsilon_\mu^*(k).
\end{aligned} \tag{16}$$

Using this general amplitude for a three-body pseudoscalar decay, $P\to\gamma\ell_1\bar{\ell}_2$, we calculate a general differential decay rate, which depends on the same scalar functions $A_i^{P\ell_1\ell_2}(p^2,\ldots)$,

$$\begin{aligned}
\frac{d\Gamma}{dm_{12}^2 dm_{23}^2} = \frac{1}{(2\pi)^3}\frac{1}{384m_P^3}\Big[&-16(A_1^2+A_2^2)(m_{13}^2(m_P^2y^2-m_{23}^2)+m_\gamma^2m_P^2(1-y^2))\\
&+2(A_3^2+A_4^2)(m_P^2y^2-m_{12}^2)\left\{m_{13}^2(m_P^4y^2-m_{12}^2m_{23}^2)+m_\gamma^2\left(m_{13}^2m_{23}^2-\frac{1}{4}(m_P^2-m_{12}^2+m_\gamma^2)^2\right)\right\}\\
&+4(A_5^2+A_6^2)\{2m_P^6y^4+m_{12}^2((m_P^2y^2-m_{13}^2)^2+m_{23}^4)-m_P^2y^2(m_P^2+m_{12}^2)(m_P^2y^2+m_{23}^2-m_{13}^2)\}\\
&-(A_7^2+A_8^2)\{(2m_P^2y^2-m_{12}^2)((m_P^2y^2-m_{23}^2)^2+m_{13}^4)+m_P^2y^2(m_P^2-m_{12}^2)(m_P^2y^2-m_{23}^2+m_{13}^2)\}\\
&-8\mathrm{Re}[A_1A_3^*+A_2A_4^*]\{m_{13}^2(m_P^4y^2-m_{12}^2m_{23}^2)-\frac{1}{2}m_\gamma^2(m_P^2+m_\gamma^2-m_{12}^2)(m_P^2y^2-m_{12}^2)\}\\
&-16\mathrm{Re}[A_1A_5^*+A_2A_6^*]m_Pym_{13}^2(m_P^2-m_{12}^2)+8\mathrm{Re}[A_1A_7^*+A_2A_8^*]m_Pym_{13}^2(m_P^2y^2-m_{23}^2+m_{13}^2)\\
&+8\mathrm{Re}[A_3A_5^*+A_4A_6^*]m_Pym_{13}^2(m_P^4y^2-m_{12}^2m_{23}^2)+4\mathrm{Re}[A_3A_7^*+A_4A_8^*]m_Pym_{13}^2(m_P^4y^2-m_{12}^2m_{23}^2)\\
&+4\mathrm{Re}[A_5A_7^*+A_6A_8^*](m_P^2-m_{12}^2)(m_P^2y^2-m_{12}^2)(m_P^2y^2-m_{23}^2+m_{13}^2)\Big].
\end{aligned} \tag{17}$$

Here the Mandelstam variables have the usual definitions: $m_{12}^2=(p_1+p_2)^2$, $m_{13}^2=(p_1+k)^2$, $m_{23}^2=(p_2+k)^2$, where $p_{1,2}$ is the $\ell_{1,2}$ lepton momentum, k is the γ photon momentum, and they are related to the pseudoscalar momentum, p, by $p=p_1+p_2+k$. The mass m_P is the pseudoscalar mass, m_2 is the heavier lepton mass, and $y=m_2/m_P$. The superscript of $P\ell_1\ell_2$ on the scalar functions $A_i^{P\ell_1\ell_2}(p^2,\ldots)$ is dropped for brevity in Eq. (17). We introduce a photon mass, m_γ, to regulate the infrared divergences that will appear via bremsstrahlung diagrams. We use a value of $m_\gamma=60$ MeV as our cutoff, which is near the final state invariant mass resolution of experiments [33].

B. Scalar functions $A_i^{P\ell_1\ell_2}$ for B_q^0, $\bar{D}^0$, and K^0 mesons

The scalar functions $A_i^{P\ell_1\ell_2}(p^2,\ldots)$ introduced in Eq. (14) can only depend on kinematical invariants and form factors. These functions can be calculated on the lattice or using other nonperturbative methods. Examining the four-fermion Lagrangian of Eq. (4) one can find that the contributions of Figs. (1), (3), and (4) to $A_i^{P\ell_1\ell_2}$ could be written in terms of the form factors for $P(p)\to\gamma(k)$ transitions used to parametrize lepton flavor conserving decays, such as $P^+\to\gamma\ell^+\bar{\nu}$ or $P^0\to\gamma\ell\bar{\ell}$. These form factors are defined as [28–30,33]

$$\begin{aligned}
&\langle\gamma(k)|\bar{q}_1\gamma^\mu\gamma_5 q_2|P(p)\rangle\\
&\quad=i\sqrt{4\pi\alpha}\,\varepsilon_\alpha^*(k)[g^{\alpha\mu}p\cdot k-p^\alpha k^\mu]f_A^P[Q^2,k^2],
\end{aligned} \tag{18}$$

$$\langle\gamma(k)|\bar{q}_1\gamma^\mu q_2|P(p)\rangle=\sqrt{4\pi\alpha}\,\varepsilon_\nu^*(k)\epsilon^{\mu\nu\alpha\beta}p_\alpha k_\beta f_V^P[Q^2,k^2], \tag{19}$$

$$\begin{aligned}
&\langle\gamma^*(k)|\bar{q}_1\sigma^{\mu\nu}q_2|P(p)\rangle\\
&\quad=i\sqrt{4\pi\alpha}\,\varepsilon_\alpha^*(k)\Big[\epsilon^{\mu\nu\alpha\beta}k_\beta f_{T1}^P[Q^2,k^2]\\
&\qquad+\left(p^\alpha-\frac{p\cdot k}{k^2}k^\alpha\right)\epsilon^{\mu\nu\rho\beta}p_\rho k_\beta f_{T2}^P[Q^2,k^2]\\
&\qquad+\left(\epsilon^{\mu\nu\alpha\rho}p_\rho+\frac{k^\alpha}{k^2}\epsilon^{\mu\nu\rho\beta}p_\rho k_\beta\right)f_{T3}^P[Q^2,k^2]\Big].
\end{aligned} \tag{20}$$

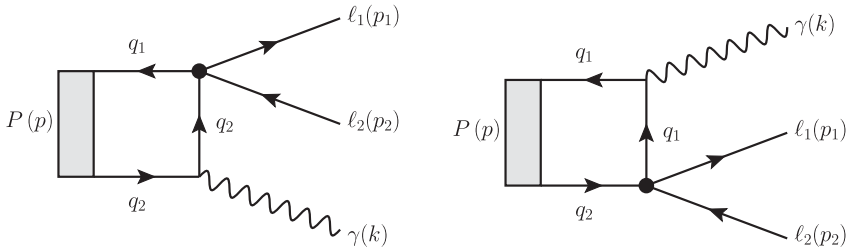

FIG. 1. Four-fermion interaction diagrams for $\mathcal{A}(P \to \gamma \ell_1 \bar{\ell}_2)$ for operators of type $\mathcal{O} \sim (\ell_1 \bar{\ell}_2)(\bar{q}_1 q_2)$ where $q_1 \neq q_2$ with photon $\gamma(k)$ attached to the valence quark. The black circles represent the four-fermion LFV vertex defined in $\mathcal{L}_{\text{eff}}$ of Eq. (4).

Here $Q = p - k$ and the tensor form factors are defined for an off-shell photon. The tensor form factors $f^P_{T1,2,3}[k_1^2, k_2^2]$ are functions of two variables: k_1, which is the momentum flowing from a vertex associated with the tensor current, and k_2, which is the momentum of the photon emitted from the valence quark of the meson. Note that for the on-shell photon $k^2 = 0$, there exist a relationship between f^P_{T2} and f^P_{T3}. Gauge invariance implies that $f^P_{T3}[Q^2, 0] = (p \cdot k) f^P_{T2}[Q^2, 0]$, so the tensor matrix element simplifies to [28]

$$\begin{aligned}\langle \gamma(k)|\bar{q}_1 \sigma_{\mu\nu} q_2|P(p)\rangle &= i\sqrt{4\pi\alpha}\, \varepsilon^{*\alpha}(k)[\epsilon_{\mu\nu\alpha\beta} k^\beta f^P_{T1}[Q^2, 0] \\ &\quad + (p_\alpha \epsilon_{\mu\nu\rho\beta} p^\rho k^\beta + p \cdot k \epsilon_{\mu\nu\alpha\beta} p^\beta) f^P_{T2}[Q^2, 0]]. \quad (21)\end{aligned}$$

Using Eqs. (18), (19), and (21) we can calculate the scalar function contributions of the axial, vector, and tensor operators from the Lagrangian in Eq. (4) of type $\mathcal{O} \sim (\ell_1 \bar{\ell}_2)(\bar{q}_1 q_2)$ where $q_1 \neq q_2$, which are found in Fig. (1). The contributions of these diagrams to the scalar functions $A_i^{P\ell_1\ell_2}$ are

$$\begin{aligned}
A_1^{1ab} &= \frac{\sqrt{4\pi\alpha}}{2\Lambda^2}(C_{VR}^{q_1q_2\ell_1\ell_2} - C_{VL}^{q_1q_2\ell_1\ell_2}) y m_P f_V^P[m_{12}^2, 0] \\
&\quad - \frac{\sqrt{4\pi\alpha}}{\Lambda^2}(C_{TR}^{q_1q_2\ell_1\ell_2} - C_{TL}^{q_1q_2\ell_1\ell_2}) y m_P m_H G_F \left(f_{T1}^P[m_{12}^2, 0] + \frac{m_P^2 - m_{12}^2}{2} f_{T2}^P[m_{12}^2, 0] \right), \\
A_3^{1ab} &= -\frac{2\sqrt{4\pi\alpha}}{\Lambda^2}(C_{TR}^{q_1q_2\ell_1\ell_2} - C_{TL}^{q_1q_2\ell_1\ell_2}) y m_P m_H G_F f_{T2}^P[m_{12}^2, 0], \\
A_5^{1ab} &= -\frac{\sqrt{4\pi\alpha}}{2\Lambda^2}(C_{AR}^{q_1q_2\ell_1\ell_2} + C_{AL}^{q_1q_2\ell_1\ell_2}) f_A^P[m_{12}^2] + \frac{\sqrt{4\pi\alpha}}{\Lambda^2}(C_{TR}^{q_1q_2\ell_1\ell_2} - C_{TL}^{q_1q_2\ell_1\ell_2}) y^2 m_P^2 m_H G_F f_{T2}^P[m_{12}^2, 0], \quad \text{and} \\
A_7^{1ab} &= \frac{\sqrt{4\pi\alpha}}{\Lambda^2}(C_{VR}^{q_1q_2\ell_1\ell_2} - C_{VL}^{q_1q_2\ell_1\ell_2}) f_V^P[m_{12}^2, 0]. \quad (22)
\end{aligned}$$

Note that in this section [e.g., in writing Eq. (22)] we suppressed the previously used superscript of $P\ell_1\ell_2$ in favor of a superscript related to the associated diagrams, which consists of the figure number and subfigure letters (i.e., $1ab$). We only show the odd subscript scalar function equations. The even subscript equations can be found from the odd subscript equations by replacing the left-handed WCs by their negative magnitudes (i.e., $C_{VL} \to -C_{VL}$, $C_{AL} \to -C_{AL}$, etc.,) and multiplying the odd subscript scalar function by the imaginary constant i. This may be used to find A_2 from A_1, A_4 from A_3, A_6 from A_5, and A_8 from A_7 and is true throughout this section.

There is no contribution in Fig. 1 from the pseudoscalar operators of the Lagrangian in Eq. (4). This can be seen by taking a matrix element of the divergence of axial current to relate the axial and pseudoscalar matrix elements,

$$\begin{aligned}\langle \gamma(k)|\bar{q}_1 \gamma_5 q_2|P(p)\rangle &= -\frac{1}{m_{q_1} + m_{q_2}} p^\mu \langle \gamma(k)|\bar{q}_1 \gamma_\mu \gamma_5 q_2|P(p)\rangle, \quad (23)\end{aligned}$$

and using Eq. (18) to get

$$\langle \gamma(k)|\bar{q}_1 \gamma_5 q_2|P(p)\rangle = 0. \quad (24)$$

A similar argument can be made to prove that the scalar operators also do not give form factor contributions.

The bremsstrahlung diagrams in Fig. 2 are calculated similarly to the two-body decays of Sec. III using the matrix element of Eq. (8). We have given the photon a small mass, m_γ, to regulate the infrared divergences. This divergence only appears in the quark flavor changing axial and pseudoscalar operator terms of the scalar functions,

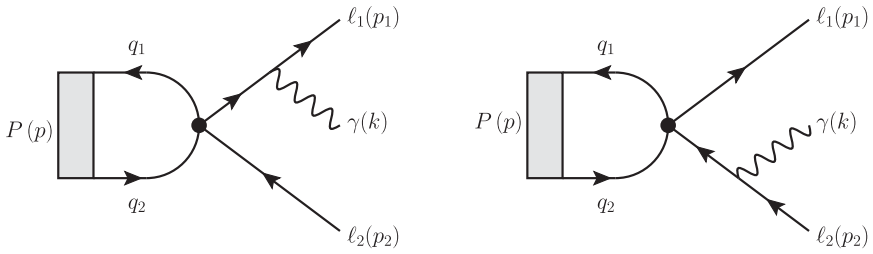

FIG. 2. Bremsstrahlung diagrams for $\mathcal{A}(P \to \gamma \ell_1 \bar{\ell}_2)$ for operators of type $\mathcal{O} \sim (\ell_1 \bar{\ell}_2)(\bar{q}_1 q_2)$ where $q_1 \neq q_2$. The black circles represent the four-fermion LFV vertex defined in $\mathcal{L}_{\text{eff}}$ of Eq. (4).

Eq. (25), so the photon mass is set to zero for the nondivergent terms. The same is true for the differential decay rate in Eq. (17). The axial and pseudoscalar operator scalar function terms are defined here as

$$A_1^{2ab} = \frac{\sqrt{4\pi\alpha}}{2\Lambda^2}(C_{AR}^{q_1q_2\ell_1\ell_2} + C_{AL}^{q_1q_2\ell_1\ell_2} + m_P^2 G_F (C_{PR}^{q_1q_2\ell_1\ell_2} + C_{PL}^{q_1q_2\ell_1\ell_2})) \times \frac{y m_P f_P (m_P^2 + m_\gamma^2 - m_{12}^2)}{m_{13}^2 (m_{23}^2 - m_P^2 y^2)},$$

$$A_3^{2ab} = \frac{2\sqrt{4\pi\alpha}}{\Lambda^2}(C_{AR}^{q_1q_2\ell_1\ell_2} - C_{AL}^{q_1q_2\ell_1\ell_2} + m_P^2 G_F (C_{PR}^{q_1q_2\ell_1\ell_2} - C_{PL}^{q_1q_2\ell_1\ell_2})) \frac{y m_P f_P}{m_{13}^2 (m_{23}^2 - m_P^2 y^2)}. \quad (25)$$

The dipole operator diagrams of Eq. (2) found in Fig. 3 contain contributions from the SM dipole penguin operator, Eq. (3). This is directly related to both the on and off-shell tensor matrix elements in Eqs. (20) and (21) from which we need to write matrix elements of the form $\langle \gamma(k)|\bar{q}_1 \sigma^{\mu\nu}(1 \pm \gamma_5) q_2 | P(p)\rangle$. These can be found by using the relation $\sigma_{\mu\nu}\gamma_5 = -\frac{i}{2}\epsilon_{\mu\nu\alpha\beta}\sigma^{\alpha\beta}$, which yields:

$$\langle \gamma(k)|\bar{q}_1 \sigma^{\mu\nu}(1 \pm \gamma_5) q_2 | P(p)\rangle Q_\nu = i\sqrt{4\pi\alpha}\, \varepsilon_\alpha^*(k)\{(f_{T1}^P[Q^2,0] + p\cdot k f_{T2}^P[Q^2,0])\epsilon^{pk\alpha\mu} \pm i(f_{T1}^P[Q^2,0] + p\cdot Q f_{T2}^P[Q^2,0])(g^{\alpha\mu} p\cdot k - p^\alpha k^\mu)\}, \quad (26)$$

$$\langle \gamma^*(Q)|\bar{q}_1 \sigma^{\mu\nu}(1 \pm \gamma_5) q_2 | P(p)\rangle k_\nu = f i\sqrt{4\pi\alpha}\, \varepsilon_\alpha^*(Q)\{\epsilon^{pk\mu\alpha} \pm i(g^{\alpha\mu} p\cdot k - p^\mu k^\alpha)\} \times (f_{T1}^P[0,Q^2] + f_{T3}^P[0,Q^2]). \quad (27)$$

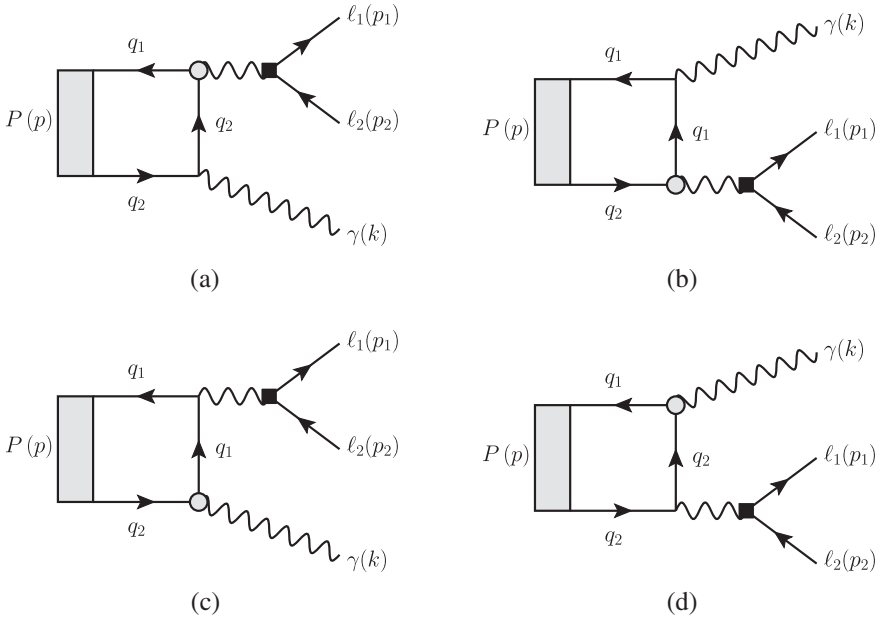

FIG. 3. Dipole operator diagrams for $\mathcal{A}(P \to \gamma \ell_1 \bar{\ell}_2)$. The grey circles with the black border represent the SM dipole penguin vertex (Eq. (3)) and the black boxes represent the dipole LFV vertex [Eq. (2)]. Note that the contributions of these diagrams are severely constrained by already available data on $\ell_1 \to \ell_2 \gamma$ decays.

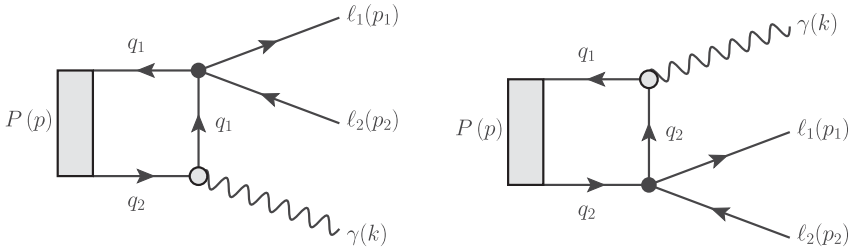

FIG. 4. Four-fermion interaction diagrams for $\mathcal{A}(P \to \gamma \ell_1 \bar{\ell}_2)$ for operators of type $\ell_1 \bar{\ell}_2 \bar{q} q$ with photon $\gamma(k)$ attached to the SM dipole penguin vertex. The black circles represent the four-fermion LFV vertex [Eq. (4)] and the grey circles with the black border represent the SM dipole penguin vertex [Eq. (3)].

The on-shell matrix element in Eq. (26) contributes to Figs. 3(a) and 3(b). While the off-shell matrix element in Eq. (27) is necessary for calculating the dipole operator contributions of the diagrams in Figs. 3(c) and 3(d). In these diagrams, the lepton current is attached to the photon coming from the meson's valence quarks and so $Q \leftrightarrow k$ when we calculate Eq. (27). Using these matrix elements we find the dipole operator components of the scalar functions which are

$$
\begin{aligned}
A_1^{3abcd} &= -\frac{1}{\Lambda^2}(C_{DR}^{\ell_1\ell_2} - C_{DL}^{\ell_1\ell_2})\frac{4\pi\alpha}{\pi^2} y m_P m_H \frac{G_F}{\sqrt{2}} C_{7\gamma} \sum_q \lambda_q f_{T,I}^P, \\
A_3^{3abcd} &= \frac{2}{\Lambda^2}\frac{4\pi\alpha}{\pi^2}\frac{y m_P m_H}{m_{12}^2}\frac{G_F}{\sqrt{2}} C_{7\gamma} \sum_q \lambda_q ((C_{DR}^{\ell_1\ell_2} - C_{DL}^{\ell_1\ell_2}) f_{T,\mathrm{I}}^P - (C_{DR}^{\ell_1\ell_2} + C_{DL}^{\ell_1\ell_2}) f_{T,\mathrm{II}}^P), \\
A_5^{3abcd} &= -\frac{1}{\Lambda^2}\frac{4\pi\alpha}{\pi^2}\frac{y^2 m_P^2 m_H}{m_{12}^2}\frac{G_F}{\sqrt{2}} C_{7\gamma} \sum_q \lambda_q ((C_{DR}^{\ell_1\ell_2} - C_{DL}^{\ell_1\ell_2}) f_{T,\mathrm{I}}^P - (C_{DR}^{\ell_1\ell_2} + C_{DL}^{\ell_1\ell_2}) f_{T,\mathrm{II}}^P),
\end{aligned} \tag{28}
$$

where we have used the shorthand notations $f_{T,\mathrm{I}}^P$ and $f_{T,\mathrm{II}}^P$ that we define as

$$
\begin{aligned}
f_{T,\mathrm{I}}^P &= f_{T1}^P[m_{12}^2, 0] + f_{T1}^P[0, m_{12}^2] + \frac{m_P^2 - m_{12}^2}{2} f_{T2}^P[m_{12}^2, 0] + f_{T3}^P[0, m_{12}^2] \quad \text{and} \\
f_{T,\mathrm{II}}^P &= f_{T1}^P[m_{12}^2, 0] + f_{T1}^P[0, m_{12}^2] + \frac{m_P^2 + m_{12}^2}{2} f_{T2}^P[m_{12}^2, 0] + f_{T3}^P[0, m_{12}^2].
\end{aligned} \tag{29}
$$

So far we have not addressed the contributions of the diagrams in Fig. 4. These diagrams contain contributions from the axial, vector, and tensor operators from the Lagrangian in Eq. (4) of type $\ell_1 \bar{\ell}_2 \bar{q} q$, where the quarks are both the same flavor. As was the case for the four-fermion operators that had a flavor change on both the quark side and lepton side, the scalar and pseudoscalar operators do not contribute. We can calculate the contributions of the vector operators using the same tensor matrix element as in Eq. (27), but with one important modification. The form factors are the sum of two form factors related to each quark flavor, $f_{Ti} = \tilde{f}_{Ti}^{q_1} + \tilde{f}_{Ti}^{q_2}$ (e.g., see [40]). For convenience we will use a definition with the quark charge explicitly included in the formula, $f_{Ti} = Q_{q_1} f_{Ti}^{q_1} + Q_{q_2} f_{Ti}^{q_2}$. This is important because in the case of Fig. 4(a) we only have contributions from $f_{Ti}^{q_1}$ and in Fig. 4(b) we only have $f_{Ti}^{q_2}$.

$$
\begin{aligned}
A_1^{4ab} &= -\frac{\sqrt{4\pi\alpha}}{\pi^2\Lambda^2}\sum_{j=1}^{2}(C_{VR}^{q_j\ell_1\ell_2} - C_{VL}^{q_j\ell_1\ell_2})\frac{y m_P}{2}\frac{G_F}{\sqrt{2}} C_{7\gamma}\sum_q \lambda_q^P (f_{T1}^{P,q_j}[0, m_{12}^2] + f_{T3}^{P,q_j}[0, m_{12}^2]), \\
A_5^{4ab} &= \frac{\sqrt{4\pi\alpha}}{\pi^2\Lambda^2}\sum_{j=1}^{2}(C_{VR}^{q_j\ell_1\ell_2} + C_{VL}^{q_j\ell_1\ell_2})\frac{m_H}{2}\frac{G_F}{\sqrt{2}} C_{7\gamma}\sum_q \lambda_q^P (f_{T1}^{P,q_j}[0, m_{12}^2] + f_{T3}^{P,q_j}[0, m_{12}^2]), \\
A_7^{4ab} &= -\frac{\sqrt{4\pi\alpha}}{\pi^2\Lambda^2}\sum_{j=1}^{2}(C_{VR}^{q_j\ell_1\ell_2} - C_{VL}^{q_j\ell_1\ell_2}) m_H \frac{G_F}{\sqrt{2}} C_{7\gamma}\sum_q \lambda_q^P (f_{T1}^{P,q_j}[0, m_{12}^2] + f_{T3}^{P,q_j}[0, m_{12}^2]).
\end{aligned} \tag{30}
$$

TABLE IV. Upper limits on $B_q^0 \to \gamma \ell_1 \bar{\ell}_2$ branching ratios from known Wilson coefficient constraints using form factors for four-fermion axial and pseudoscalar operators of type $\mathcal{O} \sim (\ell_1 \bar{\ell}_2)(\bar{q}_1 q_2)$ where $q_1 \neq q_2$.

	Upper limits			
Wilson coefficient	$\mathcal{B}(B_d^0 \to \gamma\mu\tau)$	$\mathcal{B}(B_d^0 \to \gamma e\tau)$	$\mathcal{B}(B_d^0 \to \gamma e\mu)$	$\mathcal{B}(B_s^0 \to \gamma e\mu)$
$C_{AR}^{qb\ell_1\ell_2}$	9.2×10^{-7}	1.2×10^{-6}	6.5×10^{-11}	3.7×10^{-10}
$C_{AL}^{qb\ell_1\ell_2}$	9.2×10^{-7}	1.2×10^{-6}	6.5×10^{-11}	3.7×10^{-10}
$C_{PR}^{qb\ell_1\ell_2}$	9.0×10^{-7}	1.2×10^{-6}	3.2×10^{-11}	1.7×10^{-10}
$C_{PL}^{qb\ell_1\ell_2}$	9.0×10^{-7}	1.2×10^{-6}	3.2×10^{-11}	1.7×10^{-10}

TABLE V. Upper limits on $\bar{D}^0(u\bar{c})$, $K_L^0((d\bar{s} - s\bar{d})/\sqrt{2}) \to \gamma \ell_1 \bar{\ell}_2$ branching ratios from known Wilson coefficient constraints using form factors for four-fermion axial and pseudoscalar operators of type $\mathcal{O} \sim (\ell_1 \bar{\ell}_2)(\bar{q}_1 q_2)$ where $q_1 \neq q_2$. Note the K_L^0 results are for short distance (SD) interactions.

Wilson	Upper limits	
coefficient	$\mathcal{B}(\bar{D}^0 \to \gamma e\mu)$	$\mathcal{B}(K_L^0 \to \gamma e\mu)_{SD}$
$C_{AR}^{q_1 q_2 \ell_1 \ell_2}$	2.2×10^{-10}	2.3×10^{-14}
$C_{AL}^{q_1 q_2 \ell_1 \ell_2}$	2.2×10^{-10}	2.3×10^{-14}
$C_{PR}^{q_1 q_2 \ell_1 \ell_2}$	4.5×10^{-9}	2.2×10^{-14}
$C_{PL}^{q_1 q_2 \ell_1 \ell_2}$	4.5×10^{-9}	2.2×10^{-14}

Applying this information to the decays of B_q^0, $\bar{D}^0$, and K^0 mesons shown in Figs. 1–4, we find that each scalar function $A_i^{P\ell_1\ell_2}$ is written as

$$A_i^{P\ell_1\ell_2}(p^2, \ldots) = A_i^{1ab} + A_i^{2ab} + A_i^{3abcd} + A_i^{4ab} \quad (i = 1-8), \tag{31}$$

which are functions of model independent form factors and decay constants.

IV. RESULTS

Unfortunately, no experimental limits on the branching ratios of radiative lepton-flavor violating decays exist to constrain all of the applicable Wilson coefficients of the effective Lagrangian of Eq. (1). We encourage our colleagues from the LHC and KEK to study these decays. However, some information about Wilson coefficients is available from other transitions, such as two-body decays discussed in Sec. III. In this section we use this information, along with the assumption of single operator dominance to derive the expectations for the size of the radiative LFV decays, if driven by those operators. These upper limits are presented in Tables IV and V and the differential decay rates are plotted in Figs. 5–8 of Sec. IV A.

All of the form factors and numerical constants, unless previously mentioned, used to obtain the results in this section may be found in Appendix A. In some cases where form factors are currently unknown, we apply a constituent quark model to estimate the relevant contribution. The quark model approach and results may be found in Appendix B.

A. Spectra

Inputting the scalar functions of Eq. (31) in the differential decay rate, Eq. (17), and integrating over the Mandelstam variables m_{23}^2 and m_{12}^2, we calculate the differential decay rate, $d\Gamma/dm_{12}^2$, and total decay rate, $\Gamma(P \to \gamma \ell_1 \bar{\ell}_2)$. Using these results we may predict the differential decay spectra for individual operators, $(1/\Gamma)(d\Gamma/dE_\gamma)$. Where we make the variable change from m_{12}^2 to E_γ, the photon energy in the meson rest frame, and normalize to the total decay rate. This analysis requires the practical assumption of single operator dominance so that the unknown WCs of individual operators will cancel between the differential and total decay rates.

The differential decay rates for the vector and tensor operators of type $\mathcal{O} \sim (\ell_1 \bar{\ell}_2)(\bar{q}_1 q_2)$ where $q_1 \neq q_2$ are

$$\frac{d\Gamma_V^{q_1 q_2 \ell_1 \ell_2}}{dm_{12}^2} = \frac{C_{VR}^2 + C_{VL}^2}{\Lambda^4} \frac{4\pi\alpha}{(2\pi)^3} \frac{1}{576 m_P^2} (m_P^2 - m_{12}^2)^3 \times (2m_{12}^2 - 3m_P^2 y^2) f_V^P[m_{12}^2, 0], \tag{32}$$

$$\frac{d\Gamma_T^{q_1 q_2 \ell_1 \ell_2}}{dm_{12}^2} = \frac{C_{TR}^2 + C_{TL}^2}{\Lambda^4} \frac{4\pi\alpha}{(2\pi)^3} \frac{y^2 m_{q_H}^2 G_F^2}{288 m_P^2} (m_P^2 - m_{12}^2)^3 \times ((2f_{T1}^P[m_{12}^2, 0] + m_P^2 f_{T2}^P[m_{12}^2, 0])^2 + m_{12}^2 (f_{T2}^P[m_{12}^2, 0])^2). \tag{33}$$

Here we have suppressed the superscripts of the WCs for brevity (e.g., $C_{VR}^{q_1 q_2 \ell_1 \ell_2} \to C_{VR}$). We drop terms higher in order than y^2, which is a good approximation in most cases as the ratio y is small. The vector and tensor operators with flavor change on both the quark and lepton side are of particular importance to our analysis. They cannot be constrained via two-body decays and so the three-body decay channels present us with a unique opportunity to place limits on the associated WCs. The vector operators also have an advantage over the tensor operators because they are not chirally suppressed by quark and lepton

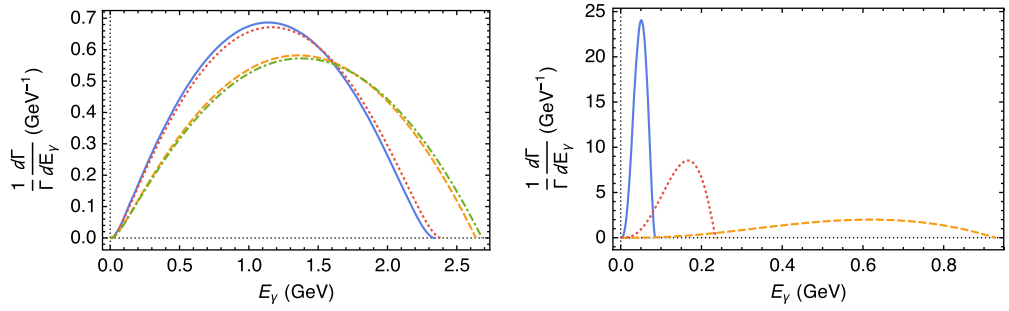

FIG. 5. Vector operator ($\mathcal{O} \sim (\ell_1 \bar{\ell}_2)(\bar{q}_1 q_2)$ where $q_1 \neq q_2$) differential decay plots as functions of photon energy E_γ: (a) $B_d \to \gamma\mu\tau$ or $\gamma e\tau$ (solid blue curve), $B_d \to \gamma e\mu$ (short-dashed gold curve), $B_s \to \gamma\mu\tau$ or $\gamma e\tau$ (dotted red curve), $B_s \to \gamma e\mu$ (dot-dashed green curve); (b) $D \to \gamma e\tau$ (solid blue curve), $D \to \gamma e\mu$ (short-dashed gold curve), $K \to \gamma e\mu$ (dotted red curve).

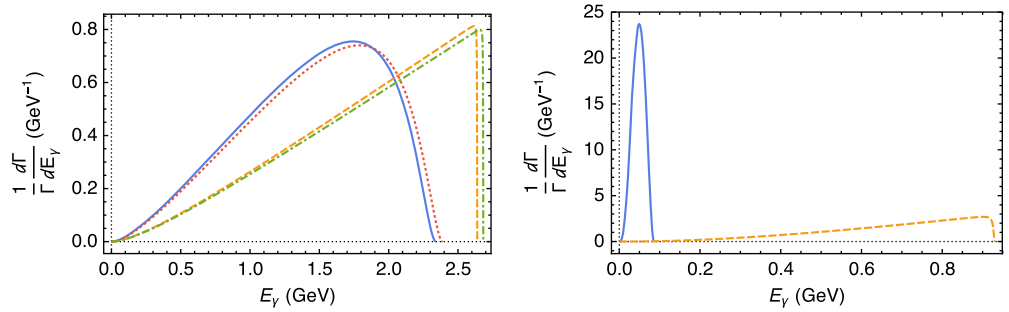

FIG. 6. Tensor operator ($\mathcal{O} \sim (\ell_1 \bar{\ell}_2)(\bar{q}_1 q_2)$ where $q_1 \neq q_2$) differential decay plots as functions of photon energy E_γ: (a) $B_d \to \gamma\mu\tau$ or $\gamma e\tau$ (solid blue curve), $B_d \to \gamma e\mu$ (short-dashed gold curve), $B_s \to \gamma\mu\tau$ or $\gamma e\tau$ (dotted red curve), $B_s \to \gamma e\mu$ (dot-dashed green curve); (b) $D \to \gamma e\tau$ (solid blue curve), $D \to \gamma e\mu$ (short-dashed gold curve).

masses. Assuming WCs are of similar size, this means the vector operators would give a larger contribution to the overall decay rate and conversely are better constrained by experimental limits. The differential spectra given in Eqs. (32) and (33) are shown in Figs. 5–6.

The three-body decays considered here also provide complementary access to the axial and pseudoscalar operators of type $\mathcal{O} \sim (\ell_1 \bar{\ell}_2)(\bar{q}_1 q_2)$ where $q_1 \neq q_2$. We do not provide the equations for the individual differential decay rates as they are more cumbersome than their vector and tensor counterparts and they are better constrained via two-body decays. Their differential spectra are plotted in Figs. 7–8 We demonstrate how well constrained these and other operators are in Sec. IV B and Appendix B 2.

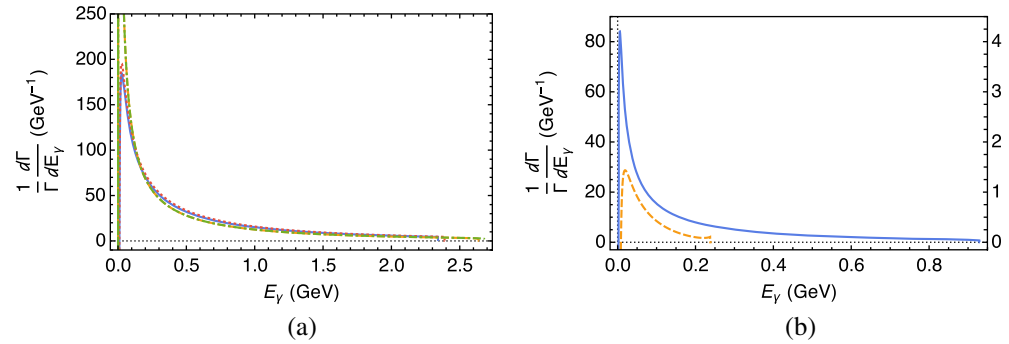

FIG. 7. Axial operator ($\mathcal{O} \sim (\ell_1 \bar{\ell}_2)(\bar{q}_1 q_2)$ where $q_1 \neq q_2$) differential decay plots as functions of photon energy E_γ: (a) $B_d \to \gamma\mu\tau$ or $\gamma e\tau$ (solid blue curve), $B_d \to \gamma e\mu$ (short-dashed gold curve), $B_s \to \gamma\mu\tau$ or $\gamma e\tau$ (dotted red curve), $B_s \to \gamma e\mu$ (dot-dashed green curve); (b) left scale $D \to \gamma e\mu$ (solid blue curve), right scale $K \to \gamma e\mu$ (short-dashed gold curve).

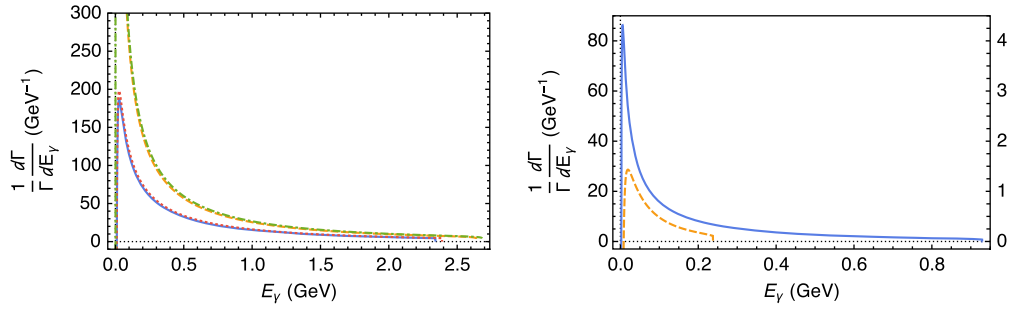

FIG. 8. Pseudoscalar operator ($\mathcal{O} \sim (\ell_1\bar{\ell}_2)(\bar{q}_1 q_2)$ where $q_1 \neq q_2$) differential decay plots as functions of photon energy E_γ: (a) $B_d \to \gamma\mu\tau$ or $\gamma e\tau$ (solid blue curve), $B_d \to \gamma e\mu$ (short-dashed gold curve), $B_s \to \gamma\mu\tau$ or $\gamma e\tau$ (dotted red curve), $B_s \to \gamma e\mu$ (dot-dashed green curve); (b) left scale $D \to \gamma e\mu$ (solid blue curve), right scale $K \to \gamma e\mu$ (short-dashed gold curve).

B. Limits

Using the available limits on Wilson coefficients from Sec. III with the form factors of Appendix A, we predict the upper threshold experiments must reach to potentially see LFV in the $P \to \gamma\ell_1\bar{\ell}_2$ decays involving the axial and pseudoscalar operators of type $\mathcal{O} \sim (\ell_1\bar{\ell}_2)(\bar{q}_1 q_2)$ where $q_1 \neq q_2$ and dipole operators. These upper bounds are presented in Table IV for B_q^0 decays and in Table V for $\bar{D}^0$ and K_L^0 decays. K_L^0 is used in lieu of K^0 for the limits on the branching ratios due to a lack of experimental information on the total decay rate of K^0. The normalized differential decay plots of K^0 are the same as K_L^0 because the normalization to the total decay rate cancels out the numerical differences (i.e., a factor of $1/\sqrt{2}$).

The predicted upper limits of the four-fermion axial and pseudoscalar operators for radiative pseudoscalar decays $P \to \gamma\ell_1\bar{\ell}_2$ in Tables IV and V demonstrate that these operators ultimately are better constrained by their two-body decay counterparts. When we compare the predicted upper bounds of three-body rates in Tables IV and V to the two-body experimental limits in Table I we see they are one to two orders of magnitude smaller. Therefore the three-body decays could still provide complimentary access to these operators.

The tensor form factors in Appendix A also allow us to analyze the contributions of the dipole operators of Eq. (2). The dipole operators are best constrained via radiative lepton decays $\ell_2 \to \ell_1\gamma$, where $\ell_2 = \tau$, μ and $\ell_1 = \mu$, e. These decays have been the focus of most LFV experiments and therefore have the best constraints: $\mathcal{B}(\tau \to \mu\gamma) = 4.4 \times 10^{-8}$, $\mathcal{B}(\tau \to e\gamma) = 3.3 \times 10^{-8}$, and $\mathcal{B}(\mu \to e\gamma) = 4.2 \times 10^{-13}$ [19,41,42]. In our previous work we were able to provide complimentary access via two-body vector quarkonium decays $V \to \gamma\ell_1\bar{\ell}_2$ [9].

Using the WC constraints obtained from the radiative lepton decays $\ell_2 \to \ell_1\gamma$ in [9], we predict the dipole operator decay upper limits for $P \to \gamma\ell_1\bar{\ell}_2$ in Table VI. Here the predicted upper limits range from 10^{-21}–10^{-38}, which is much lower than we would expect to be within experimental reach during the foreseeable future. Despite showing that $P \to \gamma\ell_1\bar{\ell}_2$ is not a useful means to constrain the dipole operators, the results in Table VI are ten or more orders of magnitude smaller than the predictions of the axial and pseudoscalar operators in Tables IV and V. This confirms that $P \to \gamma\ell_1\bar{\ell}_2$ decays are better equipped to constrain four-fermion operators. Indeed the operators in the best position to be constrained are the quark flavor changing four-fermion

TABLE VI. Upper limits on $B_q^0(q\bar{b})$, $\bar{D}^0(u\bar{c}) \to \gamma\ell_1\bar{\ell}_2$ branching ratios from known dipole Wilson coefficient constraints using form factors for dipole operators. FPS stands for "forbidden phase space."

		Predicted upper limits		
Leptons $\ell_1\ell_2$	Wilson coefficient [9] (GeV^{-2})	$\mathcal{B}(B_d^0 \to \gamma\ell_1\bar{\ell}_2)$	$\mathcal{B}(B_s^0 \to \gamma\ell_1\bar{\ell}_2)$	$\mathcal{B}(\bar{D}^0 \to \gamma\ell_1\bar{\ell}_2)$
$\mu\tau$	$\lvert C_{DR}^{\ell_1\ell_2}/\Lambda^2\rvert = 2.6 \times 10^{-10}$	3.1×10^{-28}	1.2×10^{-26}	FPS
$e\tau$	2.7×10^{-10}	3.3×10^{-28}	1.3×10^{-26}	3.8×10^{-38}
$e\mu$	3.1×10^{-7}	5.3×10^{-24}	1.2×10^{-21}	1.4×10^{-27}
$\mu\tau$	$\lvert C_{DL}^{\ell_1\ell_2}/\Lambda^2\rvert = 2.6 \times 10^{-10}$	3.1×10^{-28}	1.2×10^{-26}	FPS
$e\tau$	2.7×10^{-10}	3.3×10^{-28}	1.3×10^{-26}	3.8×10^{-38}
$e\mu$	3.1×10^{-7}	5.3×10^{-24}	1.2×10^{-21}	1.4×10^{-27}

vector operators, which see no chiral suppression via lepton or quark masses and cannot be constrained via two-body decays.

V. CONCLUSIONS

Studies of lepton flavor violating transitions are a promising path in the search for new physics. A convenient way to study new physics is to employ effective Lagrangians. All models of new physics that include flavor-violating interactions are encoded in the values of Wilson coefficients of the low energy effective Lagrangian in Eq. (1). We argued that those Wilson coefficients can be constrained through the studies of radiative B_q^0, $\bar{D}^0$, and K^0 decays to two different flavored leptons.

It is clear that studies of two-body $P \to \ell_1 \bar{\ell}_2$ decays allowed for the quantum number selection of a smaller subset of the effective operators, which reduced our reliance on single operator dominance. Yet, the radiative three-body decays to $\gamma \ell_1 \bar{\ell}_2$ allowed access to the effective operators in Eq. (1) which cannot be probed via any two-body meson decays. In addition to probing new operators, the three-body radiative transitions also allowed for complimentary access to four-fermion operators constrained by two-body decays without the need to include a composite strongly-interacting meson to the final state. Finally, we provide evidence that the dipole operators are so well constrained by radiative LFV transitions $\ell_2 \to \ell_1 \gamma$ that their threshold for contributions to $\mathcal{B}(P \to \gamma \ell_1 \bar{\ell}_2)$ is many orders of magnitude below experimental reach. Thus, their contribution to the sum of amplitudes in Eq. (31) can be safely dropped.

As more data is produced by Belle II and the LHCb experiment, we emphatically encourage our experimental colleagues to produce experimental limits on both LFV and radiative LFV decays of the B_q^0, $\bar{D}^0$, and K^0 mesons discussed in this work.

ACKNOWLEDGMENTS

We would like to thank Dmitri Melikhov and Alexander Khodjamirian for useful discussions. This work has been supported in part by the U.S. Department of Energy under Contract No. DE-SC0007983. A. A. P. thanks the University of Siegen for hospitality where part of this work was performed under Comenius Guest Professorship.

APPENDIX A: FORM FACTORS AND NUMERICAL CONSTANTS

To estimate differential decay rates and the upper limits of the total decay rates of the radiative decays in Sec. IV, we must apply the form factors of Eqs. (18)–(20) and the numerical constants of Tables VII and VIII. Numerical inputs for the CKM matrix elements are found in [19]. Before we can apply these form factors, we must relate them to those calculated in the literature, which are defined as [28–33]

TABLE VII. $\overline{\text{MS}}$ quark masses for decay calculations [19].

m_u	m_d	m_c	m_s	m_b
$2.2^{+0.6}_{-0.4}$ MeV	$4.7^{+0.5}_{-0.4}$ MeV	1.28 ± 0.03 GeV	96^{+8}_{-4} MeV	$4.18^{+0.04}_{-0.03}$ GeV

TABLE VIII. Penguin operator Wilson coefficients, $C_{7\gamma}$, for decay calculations.

Transition	Scale μ [GeV]	$\lvert C_{7\gamma}\rvert$	Ref.
$b \to d(s)\gamma$	5.0	0.299	[11]
$c \to u\gamma$	1.3	$\frac{0.0025}{4\lvert V_{ub}^* V_{cb}\rvert}$	[43]

$$
\begin{aligned}
&\langle \gamma^*(k_2)|\bar{q}_1 \gamma^\mu \gamma_5 q_2|P(p)\rangle \\
&\quad = ie\varepsilon_\alpha^*(k_2)(g^{\alpha\mu} k_1 \cdot k_2 - k_1^\alpha k_2^\mu)\frac{F_A^P[k_1^2, k_2^2]}{m_P}, \\
&\langle \gamma^*(k_2)|\bar{q}_1 \gamma^\mu q_2|P(p)\rangle \\
&\quad = e\varepsilon_\alpha^*(k_2)\epsilon^{k_1 k_2 \mu\alpha}\frac{F_V^P[k_1^2, k_2^2]}{m_P}, \\
&\langle \gamma^*(k_2)|\bar{q}_1 \sigma^{\mu\nu} \gamma_5 q_2|P(p)\rangle k_{1\nu} \\
&\quad = e\varepsilon_\alpha^*(k_2)(g^{\alpha\mu} k_1 \cdot k_2 - k_1^\alpha k_2^\mu)F_{TA}^P[k_1^2, k_2^2], \quad \text{and} \\
&\langle \gamma^*(k_2)|\bar{q}_1 \sigma^{\mu\nu} q_2|P(p)\rangle k_{1\nu} \\
&\quad = ie\varepsilon_\alpha^*(k_2)\epsilon^{k_1 k_2 \mu\alpha} F_{TV}^P[k_1^2, k_2^2].
\end{aligned} \tag{A1}
$$

These form factors are functions of two momenta, k_1, which is emitted from the $q_1 \to q_2$ weak transition current, and k_2, which is emitted from one of the valence quarks of the meson P. Here the photon is off-shell, but the on-shell definitions may be found by assuming $k_2^2 = 0$ and applying the momentum conservation relation $p = k_1 + k_2$.

Assuming $k^2 = 0$ and making the appropriate substitutions of $Q = p - k$ and k for k_1 and k_2 we find the necessary relations between the form factors in Eqs. (18)–(20) and Eq. (A1) as

$$
\begin{aligned}
F_{V,A}^P[Q^2, 0] &= m_p f_{V,A}^P[Q^2, 0], \\
F_{TV}^P[Q^2, 0] &= -f_{T1}^P[Q^2, 0] - p \cdot k f_{T2}^P[Q^2, 0], \\
F_{TA}^P[Q^2, 0] &= -f_{T1}^P[Q^2, 0] - p \cdot Q f_{T2}^P[Q^2, 0], \\
F_{TV,TA}^P[0, Q^2] &= -f_{T1}^P[0, Q^2] - f_{T3}^P[0, Q^2].
\end{aligned} \tag{A2}
$$

To make use of these relations we employ the parametrizations of [28] for the F_V, F_A, F_{TV}, and F_{TA} form factors. For the $B_q^0 \to \gamma$ form factor parametrization when

TABLE IX. Parameters of the $B_q^0 \to \gamma$ form factors, as defined in Eq. (A3) [28].

	Parameter	F_V	F_{TV}	F_A	F_{TA}
$B_{d,s}^0 \to \gamma$	$\beta(\mathrm{GeV}^{-1})$	0.28	0.30	0.26	0.33
	$\Delta(\mathrm{GeV})$	0.04	0.04	0.30	0.30

the photon γ is emitted from the valence quarks ($k_1 = Q$, $k_2 = k$) we use

$$F_i^{B_q}[E] = \beta_i \frac{f_P m_P}{\Delta_i + E_\gamma}, \quad i = \mathrm{V, A, TV, TA} \tag{A3}$$

where E_γ is the photon energy in the P-meson rest-frame. The constants β and Δ are numerical parameters which can be found in Table IX.

For the parametrization of the $\bar{D}^0, K^0 \to \gamma$ form factors when the photon γ is emitted from the valence quarks ($k_1 = Q$, $k_2 = k$) we use

$$F_i^P[m_{12}^2] = \frac{Q_{q_1} F_i^{(q_1)}[0] + Q_{q_2} F_i^{(q_2)}[0]}{1 - \frac{m_{12}^2}{M_i^2}}, \quad i = \mathrm{V, A, TV, TA}. \tag{A4}$$

Here $Q_{d(s)} = -\frac{1}{3}$, $Q_{u(c)} = \frac{2}{3}$, and the remaining parameters are found in Table X [33].

The form factors $F_{TV,TA}^P[0, Q^2]$ for B_q^0 and $\bar{D}^0$ decays are parametrized using vector meson dominance in [30,31], which gives

$$F_{TV,TA}^P[0, Q^2] = F_{TV,TA}^P[0,0] - \sum_V 2 f_V g[0]_+^{P \to V} \frac{Q^2/m_V}{Q^2 - m_V^2 + i m_V \Gamma_V}. \tag{A5}$$

The vector meson dominance input parameter values are found in Table XI. The ρ and ω mesons are part of the vector meson sum for B_d^0 and $\bar{D}^0$ form factors because of their respective d and u valence quark content. The ϕ meson is part of the vector meson sum for the B_s^0 form factor because of its s valence quark content. The zero momentum values of the tensor form factors are $F_{TV,TA}^{B_{d,s}^0}[0,0] = 0.115$ [28] and $F_{TV,TA}^{\bar{D}^0}[0,0] = Q_c f_{TV,TA}^c[0] + Q_u f_{TV,TA}^u[0]$.

Given these form factors and the general input values given in Tables VII and VIII we are able to plot the normalized differential decay rates and estimate the upper limits for the radiative branching ratios assuming single operator dominance in Sec. IV.

APPENDIX B: QUARK MODEL

When the necessary form factors are unavailable to take a model independent approach to the calculation of the four-fermion operator contributions of the diagrams in Fig. 4, we may choose a model dependent approach. We apply a constituent quark model to calculate the contributions of four-fermion vector, axial, and tensor operators of the type $(\ell_1 \bar{\ell}_2)(\bar{q}q)$. We constrained both the vector and tensor Wilson coefficients for these operators previously in [9]. The results are reproduced here in Table XII and can be used to find a predicted upper bound on the branching ratio of $\mathcal{B}(P \to \gamma \ell_1 \bar{\ell}_2)$ for individual operators using the single operator dominance assumption.

TABLE X. Parameters of the $\bar{D}^0, K^0 \to \gamma$ form factors, as defined in Eq. (A4) [33,44]. The K^0 tensor form factors will be calculated elsewhere.

	Parameter	V	A	TV	TA
$\bar{D}^0 \to \gamma$	$F_i^c(0)$	−0.12	0.14	−0.12	−0.12
	$F_i^u(0)$	−0.37	−0.31	−0.38	−0.38
	M_i (GeV)	2.0	2.3	2.0	2.4
$K^0 \to \gamma$	$F_i^d(0)$	−0.22	0.20	⋯	⋯
	$F_i^s(0)$	−0.18	−0.19	⋯	⋯
	M_i (GeV)	0.89	0.89	⋯	⋯

TABLE XI. Vector meson dominance input parameters for $F_{TV,TA}[0, Q^2]$ form factors.

V	$g[0]_+^{B_q^0 \to V}$	$g[0]_+^{\bar{D}^0 \to V}$	f_V (MeV)	m_V (MeV)	Γ_V (MeV)	Refs.
ρ	0.27	−0.66	154	775.26 ± 0.25	147.8 ± 0.9	[19,31,45]
ω	−0.27	−0.66	45.3	782.65 ± 0.12	8.49 ± 0.08	[19,31,45]
ϕ	−0.38		−58.8	1019.460 ± 0.016	4.247 ± 0.016	[19,31,45]

TABLE XII. Known Wilson coefficient limits from our previous work in [9]. Note the center dots denote unknown values which could be constrained via $P \to \gamma \ell_1 \bar{\ell}_2$.

	Leptons	Quark			
Wilson coefficient (GeV^{-2})	$\bar{\ell}_1\ell_2$	b	c	s	u/d
$\lvert C^{q\ell_1\ell_2}_{VL(R)}/\Lambda^2\rvert$	$\mu\tau$	3.5×10^{-6}	5.5×10^{-5}	⋯	⋯
$\lvert C^{q\ell_1\ell_2}_{VL(R)}/\Lambda^2\rvert$	$e\tau$	4.1×10^{-6}	1.1×10^{-4}	⋯	⋯
$\lvert C^{q\ell_1\ell_2}_{VL(R)}/\Lambda^2\rvert$	$e\mu$	⋯	1.0×10^{-5}	2.0×10^{-3}	⋯
$\lvert C^{q\ell_1\ell_2}_{AL(R)}/\Lambda^2\rvert$	$e\mu$	⋯	⋯	2.0×10^{-3}	3.0×10^{-3}
$\lvert C^{q\ell_1\ell_2}_{TL(R)}/\Lambda^2\rvert$	$\mu\tau$	2.8×10^{-2}	1.2	⋯	⋯
$\lvert C^{q\ell_1\ell_2}_{TL(R)}/\Lambda^2\rvert$	$e\tau$	3.2×10^{-2}	2.4	⋯	⋯
$\lvert C^{q\ell_1\ell_2}_{TL(R)}/\Lambda^2\rvert$	$e\mu$	⋯	4.8	⋯	⋯

1. Constituent quark model

The amplitude for the diagrams in Fig. 4 using this model is

$$\begin{aligned} i\mathcal{A}_{P\to\gamma\ell_1\ell_2} = -\frac{i}{\Lambda^2}\varepsilon^{*\mu}(k)\sum_{i=1}^{2}(&\bar{u}_{\ell_1}[C_{VR}^{q_i\ell_1\ell_2}\gamma^\alpha P_R + C_{VL}^{q_i\ell_1\ell_2}\gamma^\alpha P_L]v_{\ell_2}\langle 0|\bar{q}_1\Gamma^{V,q_i}_{\alpha\mu}q_2|P(p)\rangle \\ &+ \bar{u}_{\ell_1}[C_{AR}^{q_i\ell_1\ell_2}\gamma^\alpha P_R + C_{AL}^{q_i\ell_1\ell_2}\gamma^\alpha P_L]v_{\ell_2}\langle 0|\bar{q}_1\Gamma^{A,q_i}_{\alpha\mu}q_2|P(p)\rangle \\ &+ m_2 m_{q_i} G_F \bar{u}_{\ell_1}[C_{TR}^{q_i\ell_1\ell_2}\sigma^{\alpha\beta}P_L + C_{TR}^{q_i\ell_1\ell_2}\sigma^{\alpha\beta}P_R]v_{\ell_2}\langle 0|\bar{q}_1\Gamma^{T,q_i}_{\alpha\beta\mu}q_2|P(p)\rangle). \end{aligned} \tag{B1}$$

This amplitude is dependent on matrix elements of the form $\langle 0|\bar{q}_1\Gamma q_2|P\rangle$ with the matrices Γ defined for each operator ($\mathcal{O} \sim (\ell_1\bar{\ell}_2)(\bar{q}_i q_i)$, $i = 1, 2$) as

$$\begin{aligned} \Gamma^{V,q_1}_{\alpha\mu} &= i\frac{G_F}{\sqrt{2}}\frac{\sqrt{4\pi\alpha}}{\pi^2}m_{q_1}C_{7\gamma}\sum_q \lambda_q^P\gamma_\alpha\frac{x\not{p}-\not{k}+m_{q_1}}{(xp-k)^2-m_{q_1}^2}\sigma_{\mu\nu}(1+\gamma_5)k^\nu, \\ \Gamma^{A,q_1}_{\alpha\mu} &= i\frac{G_F}{\sqrt{2}}\frac{\sqrt{4\pi\alpha}}{\pi^2}m_{q_1}C_{7\gamma}\sum_q \lambda_q^P\gamma_\alpha\gamma_5\frac{x\not{p}-\not{k}+m_{q_1}}{(xp-k)^2-m_{q_1}^2}\sigma_{\mu\nu}(1+\gamma_5)k^\nu, \\ \Gamma^{T,q_1}_{\alpha\beta\mu} &= i\frac{G_F}{\sqrt{2}}\frac{\sqrt{4\pi\alpha}}{\pi^2}m_{q_1}C_{7\gamma}\sum_q \lambda_q^P\sigma_{\alpha\beta}\frac{x\not{p}-\not{k}+m_{q_1}}{(xp-k)^2-m_{q_1}^2}\sigma_{\mu\nu}(1+\gamma_5)k^\nu, \end{aligned} \tag{B2}$$

$$\begin{aligned} \Gamma^{V,q_2}_{\alpha\mu} &= i\frac{G_F}{\sqrt{2}}\frac{\sqrt{4\pi\alpha}}{\pi^2}m_{q_2}C_{7\gamma}\sum_q \lambda_q^P\sigma_{\mu\nu}(1+\gamma_5)k^\nu\frac{-(1-x)\not{p}+\not{k}+m_{q_2}}{((1-x)p-k)^2-m_{q_2}^2}\gamma_\alpha, \\ \Gamma^{A,q_2}_{\alpha\mu} &= i\frac{G_F}{\sqrt{2}}\frac{\sqrt{4\pi\alpha}}{\pi^2}m_{q_2}C_{7\gamma}\sum_q \lambda_q^P\sigma_{\mu\nu}(1+\gamma_5)k^\nu\frac{-(1-x)\not{p}+\not{k}+m_{q_2}}{((1-x)p-k)^2-m_{q_2}^2}\gamma_\alpha\gamma_5, \quad \text{and} \\ \Gamma^{T,q_2}_{\alpha\beta\mu} &= i\frac{G_F}{\sqrt{2}}\frac{\sqrt{4\pi\alpha}}{\pi^2}m_{q_2}C_{7\gamma}\sum_q \lambda_q^P\sigma_{\mu\nu}(1+\gamma_5)k^\nu\frac{-(1-x)\not{p}+\not{k}+m_{q_2}}{((1-x)p-k)^2-m_{q_2}^2}\sigma_{\alpha\beta}. \end{aligned} \tag{B3}$$

In modeling the quark-antiquark distribution, we chose to follow [46–48], where we can write the wave function of the ground state, $P(p)$, as

$$\psi_P = \frac{I_c}{\sqrt{6}}\phi_P[x]\gamma_5(\not{p} + m_P g[x]). \tag{B4}$$

TABLE XIII. Constituent quark masses used in calculations of quark model matrix element [49].

Quark	m_u	m_d	m_s	m_c	m_b
Constituent mass (MeV)	335.5	339.5	486	1550	4730

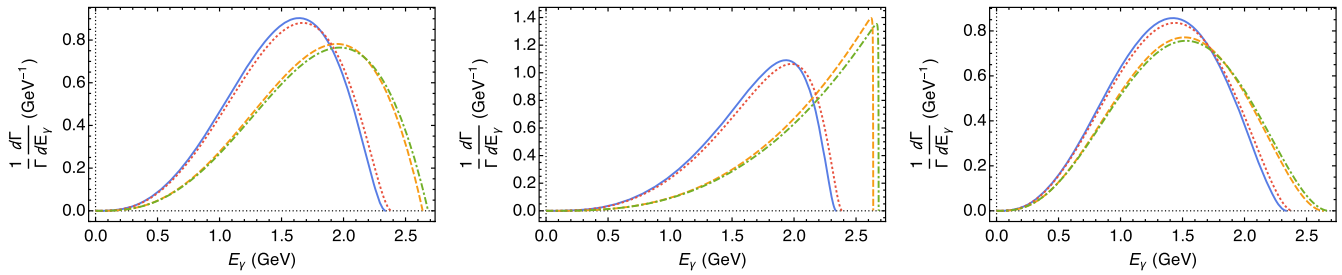

FIG. 9. Differential decay plots as functions of photon energy E_γ for (a) vector/axial, (b) left-handed tensor, and (c) right-handed tensor operators of the type $\mathcal{O} \sim (\ell_1 \bar{\ell}_2)(\bar{b}b)$. Plotted decay rates are $B_d \to \gamma\mu\tau$ or $\gamma e\tau$ (solid blue curve), $B_d \to \gamma e\mu$ (short-dashed gold curve), $B_s \to \gamma\mu\tau$ or $\gamma e\tau$ (dotted red curve), $B_s \to \gamma e\mu$ (dot-dashed green curve).

The variable x is the momentum fraction of one of the quarks and I_c is the identity matrix of color space. We have assigned the momenta in Fig. (4) such that the valence quark $\bar{q}_1$ has momentum xP and the valence quark q_2 has momentum $(1-x)P$. The function $g_P[x]$ is $g_H[x] \sim 1$ for heavy mesons and $g_L[x] = 0$ for light mesons. The distribution amplitudes used for light and heavy mesons and their normalization are

$$\begin{aligned} \phi_L &\sim x(1-x), \\ \phi_H &\sim \left[\frac{m_{q_L}}{M_H}\frac{1}{1-x} + \frac{1}{x} - 1\right]^{-2}, \\ \frac{f_P}{2\sqrt{6}} &= \int_0^1 \phi[x]dx. \end{aligned} \tag{B5}$$

Here m_{q_L} is the mass of the light quark and the normalization is related to the decay constant f_P. By taking the trace and integrating over the momentum fraction we find the matrix element

$$\langle 0|\bar{q}_1 \Gamma^\mu q_2|P\rangle = \int_0^1 \mathrm{Tr}[\Gamma^\mu \psi_P]dx. \tag{B6}$$

2. Spectra and limits

Since we applied a constituent quark model to calculate the transition amplitudes we need to define its parameters (constituent quark mass) that are used to calculate the matrix element in Eq. (B6). These masses are in Table XIII. Using this matrix element and integrating over the Mandelstam variables m_{23}^2 and m_{12}^2 we can calculate the differential decay rate as a function of the photon energy, E_γ, in the rest-frame of the meson P and the total decay rate. An example plot for these differential decay spectra normalized to the total decay

TABLE XIV. Upper limits on $B_q^0(q\bar{b}) \to \gamma\ell_1\bar{\ell}_2$ branching ratios from known Wilson coefficient constraints using constituent quark model. The center dots indicate no Wilson coefficient constraints were available for a prediction of an upper bound. Experimental studies of this decay channel would present an opportunity to constrain these Wilson coefficients.

	Upper limits					
Wilson coefficient	$\mathcal{B}(B_d^0 \to \gamma\mu\tau)$	$\mathcal{B}(B_d^0 \to \gamma e\tau)$	$\mathcal{B}(B_d^0 \to \gamma e\mu)$	$\mathcal{B}(B_s^0 \to \gamma\mu\tau)$	$\mathcal{B}(B_s^0 \to \gamma e\tau)$	$\mathcal{B}(B_s^0 \to \gamma e\mu)$
$C_{VR}^{b\ell_1\ell_2}$	5.7×10^{-20}	7.8×10^{-20}	⋯	1.8×10^{-18}	2.5×10^{-18}	⋯
$C_{VL}^{b\ell_1\ell_2}$	5.7×10^{-20}	7.8×10^{-20}	⋯	1.8×10^{-18}	2.5×10^{-18}	⋯
$C_{VR}^{q\ell_1\ell_2}$	⋯	⋯	⋯	⋯	⋯	1.3×10^{-10}
$C_{VL}^{q\ell_1\ell_2}$	⋯	⋯	⋯	⋯	⋯	1.3×10^{-10}
$C_{AR}^{q\ell_1\ell_2}$	⋯	⋯	2.0×10^{-12}	⋯	⋯	1.5×10^{-11}
$C_{AL}^{q\ell_1\ell_2}$	⋯	⋯	2.0×10^{-12}	⋯	⋯	1.5×10^{-11}
$C_{TR}^{b\ell_1\ell_2}$	3.9×10^{-21}	5.1×10^{-21}	⋯	2.1×10^{-19}	2.8×10^{-19}	⋯
$C_{TL}^{b\ell_1\ell_2}$	1.1×10^{-18}	1.5×10^{-18}	⋯	3.9×10^{-17}	5.1×10^{-17}	⋯

rate is Fig. 9, which shows the spectra of B_q^0 decays for the vector, axial, and tensor operators of type $(\ell_1\bar{\ell}_2)(\bar{q}q)$. The normalization cancels out sources of uncertainty such as the Wilson coefficients (i.e., $C_{VR(L)}^{q_i\ell_1\ell_2}$) and the CKM matrix element values. As we did in Sec. IV B, we apply known Wilson coefficient constraints from Table. XII and the single operator dominance assumption to the total decay rate to make predictions of the branching ratio upper limit for these operators, which can be found in Tables. XIV and XV.

These limits range in order of magnitude from 10^{-10}–10^{-28} and therefore many are below experimental reach. It is the spaces between these limits that should draw the reader's attention. There is much opportunity here to constrain the operators whose limits cannot be predicted. Providing limits using these RLFV decays would of course be complementary to two-body LFV decays of quarkonia (e.g., [9]), but would come for free as we constrain the vector and tensor operators with flavor changes on both the quark and lepton sides.

TABLE XV. Upper limits on $\bar{D}^0(u\bar{c}) \to \gamma\ell_1\bar{\ell}_2$ branching ratios from known Wilson coefficient constraints using constituent quark model. The center dots indicate no Wilson coefficient constraints were available for a prediction of an upper bound. Experimental studies of this decay channel would present an opportunity to constrain these Wilson coefficients.

	Upper limits	
Wilson coefficient	$\mathcal{B}(\bar{D}^0 \to \gamma e\tau)$	$\mathcal{B}(\bar{D}^0 \to \gamma e\mu)$
$C_{VR}^{c\ell_1\ell_2}$	5.1×10^{-28}	8.8×10^{-24}
$C_{VL}^{c\ell_1\ell_2}$	5.1×10^{-28}	8.8×10^{-24}
$C_{AR}^{u\ell_1\ell_2}$	⋯	1.3×10^{-16}
$C_{AL}^{u\ell_1\ell_2}$	⋯	1.3×10^{-16}
$C_{TR}^{c\ell_1\ell_2}$	6.0×10^{-28}	2.5×10^{-24}
$C_{TL}^{c\ell_1\ell_2}$	6.2×10^{-27}	3.7×10^{-22}

[1] M. Raidal *et al.*, Flavour physics of leptons and dipole moments, Eur. Phys. J. C **57**, 13 (2008).

[2] H. K. Dreiner, G. Polesello, and M. Thormeier, Bounds on broken R parity from leptonic meson decays, Phys. Rev. D **65**, 115006 (2002).

[3] H. K. Dreiner, M. Kramer, and B. O'Leary, Bounds on R-parity violating supersymmetric couplings from leptonic and semi-leptonic meson decays, Phys. Rev. D **75**, 114016 (2007).

[4] K. S. Sun, T. F. Feng, T. J. Gao, and S. M. Zhao, Search for lepton flavor violation in supersymmetric models via meson decays, Nucl. Phys. **B865**, 486 (2012).

[5] M. Lindner, M. Platscher, and F. S. Queiroz, A call for new physics: The muon anomalous magnetic moment and lepton flavor violation, Phys. Rep. **731**, 1 (2018).

[6] A. Crivellin, D. Mueller, A. Signer, and Y. Ulrich, Correlating lepton flavour (universality) violation in B decays with $\mu \to e\gamma$ using leptoquarks, Phys. Rev. D **97**, 015019 (2018).

[7] A. D. Smirnov, Vector leptoquark mass limits and branching ratios of $K_L^0, B^0, B_s \to l_i^+ l_j^-$ decays with account of fermion mixing in leptoquark currents, Mod. Phys. Lett. A **33**, 1850019 (2018).

[8] A. A. Petrov and A. E. Blechman, *Effective Field Theories* (World Scientific Publishing, Singapore, 2016), ISBN: 978-981-4434-92-8.

[9] D. E. Hazard and A. A. Petrov, Lepton flavor violating quarkonium decays, Phys. Rev. D **94**, 074023 (2016).

[10] A. Celis, V. Cirigliano, and E. Passemar, Model-discriminating power of lepton flavor violating τ decays, Phys. Rev. D **89**, 095014 (2014).

[11] G. Buchalla, A. J. Buras, and M. E. Lautenbacher, Weak decays beyond leading logarithms, Rev. Mod. Phys. **68**, 1125 (1996).

[12] V. Cirigliano, G. Ecker, H. Neufeld, A. Pich, and J. Portoles, Kaon decays in the standard model, Rev. Mod. Phys. **84**, 399 (2012).

[13] W. Altmannshofer, C. Niehoff, and D. M. Straub, $B_s \to \mu^+\mu^-$ as current and future probe of new physics, J. High Energy Phys. 05 (2017) 076.

[14] M. Beneke, C. Bobeth, and R. Szafron, Enhanced electromagnetic correction to the rare B-meson decay $B_{s,d} \to \mu^+\mu^-$, Phys. Rev. Lett. **120**, 011801 (2018).

[15] T. Blake, G. Lanfranchi, and D. M. Straub, Rare B decays as tests of the standard model, Prog. Part. Nucl. Phys. **92**, 50 (2017).

[16] C. Bobeth, M. Gorbahn, T. Hermann, M. Misiak, E. Stamou, and M. Steinhauser, $B_{s,d} \to l^+l^-$ in the Standard Model with Reduced Theoretical Uncertainty, Phys. Rev. Lett. **112**, 101801 (2014).

[17] C. Bobeth, M. Gorbahn, and E. Stamou, Electroweak corrections to $B_{s,d} \to \ell^+\ell^-$, Phys. Rev. D **89**, 034023 (2014).

[18] Y. Amhis *et al.*, Averages of b-hadron, c-hadron, and τ-lepton properties as of summer 2016, Eur. Phys. J. C **77**, 895 (2017).

[19] C. Patrignani *et al.* (Particle Data Group), Review of particle physics, Chin. Phys. C **40**, 100001 (2016) and 2017 update.

[20] A. A. Petrov and D. V. Zhuridov, Lepton flavor-violating transitions in effective field theory and gluonic operators, Phys. Rev. D **89**, 033005 (2014).

[21] B. Aubert *et al.* (*BABAR* Collaboration), Searches for the decays $B^0 \to \ell^{\pm}\tau^{\mp}$ and $B^+ \to \ell^+\nu$ ($\ell = e, \mu$) using hadronic tag reconstruction, Phys. Rev. D **77**, 091104 (2008).

[22] R. Aaij *et al.* (LHCb Collaboration), Search for the lepton-flavour violating decay $D^0 \to e^{\pm}\mu^{\mp}$, Phys. Lett. B **754**, 167 (2016).

[23] D. Ambrose *et al.* (BNL Collaboration), New Limit on Muon and Electron Lepton Number Violation from $K_L^0 \to \mu^{\pm}e^{\mp}$ Decay, Phys. Rev. Lett. **81**, 5734 (1998).

[24] R. Aaij *et al.* (LHCb Collaboration), Search for the lepton-flavour violating decays ${B_{(s)}}^0 \to e^{\pm}\mu^{\mp}$, J. High Energy Phys. 03 (2018) 078.

[25] R. J. Dowdall, C. T. H. Davies, R. R. Horgan, C. J. Monahan, and J. Shigemitsu (HPQCD Collaboration), B-Meson Decay Constants from Improved Lattice Nonrelativistic QCD with Physical u, d, s, and c Quarks, Phys. Rev. Lett. **110**, 222003 (2013).

[26] N. Carrasco *et al.*, Leptonic decay constants f_K, f_D, and f_{D_s} with $N_f = 2 + 1 + 1$ twisted-mass lattice QCD, Phys. Rev. D **91**, 054507 (2015).

[27] Y. G. Aditya, K. J. Healey, and A. A. Petrov, Faking $B_s \to \mu^+\mu^-$, Phys. Rev. D **87**, 074028 (2013).

[28] F. Kruger and D. Melikhov, Gauge invariance and form-factors for the decay $B \to \gamma l + l-$, Phys. Rev. D **67**, 034002 (2003).

[29] D. Melikhov, A. Kozachuk, and N. Nikitin, Rare FCNC radiative leptonic decays $B \to \gamma\ell^+\ell^-$, Proc. Sci., EPS-HEP2017 (**2017**) 228, [arXiv:1710.02719].

[30] A. Kozachuk, D. Melikhov, and N. Nikitin, Rare radiative leptonic B-decays, EPJ Web Conf. **125**, 02015 (2016).

[31] D. Melikhov and N. Nikitin, Rare radiative leptonic decays $B(d, s) \to l^+l^-\gamma$, Phys. Rev. D **70**, 114028 (2004).

[32] D. Guadagnoli, M. Reboud, and R. Zwicky, $B_s^0 \to \ell^+\ \ell^-\gamma$ as a test of lepton flavor universality, J. High Energy Phys. 11 (2017) 184.

[33] D. Guadagnoli, D. Melikhov, and M. Reboud, More lepton flavor violating observables for LHCb's Run 2, Phys. Lett. B **760**, 442 (2016).

[34] S. L. Glashow, D. Guadagnoli, and K. Lane, Lepton Flavor Violation in B Decays?, Phys. Rev. Lett. **114**, 091801 (2015).

[35] W. A. Bardeen and W. K. Tung, Invariant amplitudes for photon processes, Phys. Rev. **173**, 1423 (1968); Invariant amplitudes for photon processes, Phys. Rev. D **4**, 3229 (1971).

[36] H. W. Fearing, G. R. Goldstein, and M. J. Moravcsik, Amplitude structure of off-shell processes, Phys. Rev. D **29**, 2612 (1984).

[37] M. D. Scadron and H. F. Jones, Covariant M functions for higher spin, Phys. Rev. **173**, 1734 (1968).

[38] M. Jacob and G. C. Wick, On the general theory of collisions for particles with spin, Ann. Phys. (N.Y.) **7**, 404 (1959); On the general theory of collisions for particles with spin, Ann. Phys. (N.Y.) **281**, 774 (2000).

[39] G. C. Wick, Angular momentum states for three relativistic particles, Ann. Phys. (N.Y.) **18**, 65 (1962).

[40] M. Beyer, D. Melikhov, N. Nikitin, and B. Stech, Weak annihilation in the rare radiative $B \to \rho\gamma$ decay, Phys. Rev. D **64**, 094006 (2001).

[41] A. M. Baldini *et al.* (MEG Collaboration), Search for the lepton flavour violating decay $\mu^+ \to e^+\gamma$ with the full dataset of the MEG experiment, Eur. Phys. J. C **76**, 434 (2016).

[42] B. Aubert *et al.* (*BABAR* Collaboration), Searches for Lepton Flavor Violation in the Decays $\tau^{\pm} \to e^{\pm}\gamma$ and $\tau^{\pm} \to \mu^{\pm}\gamma$, Phys. Rev. Lett. **104**, 021802 (2010).

[43] A. Khodjamirian, T. Mannel, and A. A. Petrov, Direct probes of flavor-changing neutral currents in e^+ e-collisions, J. High Energy Phys. 11 (2015) 142.

[44] D. Melikhov$D \to \gamma$ Form Factors (private communication).

[45] D. Melikhov and B. Stech, Weak form-factors for heavy meson decays: An update, Phys. Rev. D **62**, 014006 (2000).

[46] Y. G. Aditya, K. J. Healey, and A. A. Petrov, Searching for super-WIMPs in leptonic heavy meson decays, Phys. Lett. B **710**, 118 (2012).

[47] A. Szczepaniak, E. M. Henley, and S. J. Brodsky, Perturbative QCD effects in heavy meson decays, Phys. Lett. B **243**, 287 (1990).

[48] G. P. Lepage and S. J. Brodsky, Exclusive processes in perturbative quantum chromodynamics, Phys. Rev. D **22**, 2157 (1980).

[49] M. D. Scadron, R. Delbourgo, and G. Rupp, Constituent quark masses and the electroweak standard model, J. Phys. G **32**, 735 (2006).